

NRC Publications Archive Archives des publications du CNRC

Evaluation of CFD meshing strategies for a hull with a yaw angle, based on Series 60 $C_b=0.6$ hull form Molyneux, W. D.

For the publisher's version, please access the DOI link below./ Pour consulter la version de l'éditeur, utilisez le lien DOI ci-dessous.

Publisher's version / Version de l'éditeur:

<https://doi.org/10.4224/8894893>

Technical Report (National Research Council of Canada. Institute for Ocean Technology); no. TR-2006-11, 2006

NRC Publications Archive Record / Notice des Archives des publications du CNRC :

<https://nrc-publications.canada.ca/eng/view/object/?id=03383664-a8c6-41e0-a85a-bef77944d271>

<https://publications-cnrc.canada.ca/fra/voir/objet/?id=03383664-a8c6-41e0-a85a-bef77944d271>

Access and use of this website and the material on it are subject to the Terms and Conditions set forth at

<https://nrc-publications.canada.ca/eng/copyright>

READ THESE TERMS AND CONDITIONS CAREFULLY BEFORE USING THIS WEBSITE.

L'accès à ce site Web et l'utilisation de son contenu sont assujettis aux conditions présentées dans le site

<https://publications-cnrc.canada.ca/fra/droits>

LISEZ CES CONDITIONS ATTENTIVEMENT AVANT D'UTILISER CE SITE WEB.

Questions? Contact the NRC Publications Archive team at

PublicationsArchive-ArchivesPublications@nrc-cnrc.gc.ca. If you wish to email the authors directly, please see the first page of the publication for their contact information.

Vous avez des questions? Nous pouvons vous aider. Pour communiquer directement avec un auteur, consultez la première page de la revue dans laquelle son article a été publié afin de trouver ses coordonnées. Si vous n'arrivez pas à les repérer, communiquez avec nous à PublicationsArchive-ArchivesPublications@nrc-cnrc.gc.ca.

DOCUMENTATION PAGE

REPORT NUMBER	NRC REPORT NUMBER	DATE	
TR-2006-11		May 2006	
REPORT SECURITY CLASSIFICATION		DISTRIBUTION	
Unclassified		Unlimited	
TITLE			
EVALUATION OF CFD MESHING STRATEGIES FOR A HULL WITH A YAW ANGLE, BASED ON SERIES 60 $C_B=0.6$ HULL FORM			
AUTHOR(S)			
David Molyneux			
CORPORATE AUTHOR(S)/PERFORMING AGENCY(S)			
Institute for Ocean Technology, National Research Council, St. John's, NL			
PUBLICATION			
SPONSORING AGENCY(S)			
Institute for Ocean Technology, National Research Council, St. John's, NL			
IOT PROJECT NUMBER		NRC FILE NUMBER	
42_2072_10			
KEY WORDS	PAGES	FIGS.	TABLES
RANS, CFD, Fluent, Mesh	iii, 50	38	10
SUMMARY			
<p>Commercial RANS based CFD programs have become an accepted method of making predictions of flow patterns, pressures and the forces resulting from water flow around a ship's hull. The main advantages of using a commercial code are that the user interfaces are flexible and well designed and the codes are validated by a larger number of users in many fields of fluid dynamics and thermodynamics. The disadvantages are that they are very general in their application, and may be more complicated or less reliable to use than a custom made code for a very specific application.</p> <p>The commercial RANS based CFD program used at Memorial University of Newfoundland is <i>Fluent</i> (Fluent Inc., 2005). Meshes for this program can be created in a number of different ways, but <i>Gambit</i> (Fluent Inc., 2005) is the product supplied by the same company for this purpose, and was the program used for this study.</p>			
ADDRESS	National Research Council Institute for Ocean Technology Arctic Avenue, P. O. Box 12093 St. John's, NL A1B 3T5 Tel.: (709) 772-5185, Fax: (709) 772-2462		



National Research Council Canada Conseil national de recherches
Canada

Institute for Ocean Technology Institut des technologies
océaniques

**EVALUATION OF CFD MESHING STRATEGIES
FOR A HULL WITH A YAW ANGLE,
BASED ON SERIES 60 $C_B=0.6$ HULL FORM**

TR-2006-11

David Molyneux

May 2006

TABLE OF CONTENTS

DESCRIPTION OF SERIES 60 $C_B=0.6$ MODEL EXPERIMENTS..... 4

 Pitot Tube Data for Yaw Angle of 10 Degrees..... 4

 LDV Data for Yaw Angle 35 Degrees..... 9

MESHING STRATEGIES FOR HULLS WITH YAW..... 13

 Previous CFD Solutions for Flow Around Series 60 $C_B=0.6$ Hull..... 13

 Mesh Development 13

 Tetrahedral Mesh for Series 60 $C_B=0.6$ 14

 Hexahedral Mesh for Series 60 $C_B=0.6$ 17

 CFD Solutions Obtained Using *Fluent* 20

 Discussion of Observed Flow Patterns 30

EVALUATION OF CFD SIMULATIONS USING DIFFERENT MESHING STRATEGIES AGAINST EXPERIMENT RESULTS 31

 Development of a Numerical Evaluation Method for Comparing Flow Patterns from CFD Predictions and Experiment Results..... 31

 Preliminary Processing 31

 Grid for Comparison of Data 32

 Interpolate CFD and Experiment Results on Common Grid 32

ANALYSIS OF CFD PREDICTIONS USING TETRAHEDRAL AND HEXAHEDRAL MESHES FOR SERIES 60 HULL WITH YAW ANGLES OF 10 DEGREES AND 35 DEGREES..... 37

 Yaw angle 10 degrees 37

 Yaw Angle 35 degrees 43

 Improvements to CFD Mesh..... 47

CONCLUSIONS..... 47

ACKNOWLEDGEMENTS 48

REFERENCES 49

**EVALUATION OF CFD MESHING STRATEGIES
FOR A HULL WITH A YAW ANGLE,
BASED ON SERIES 60 $C_B=0.6$ HULL FORM**

INTRODUCTION

Commercial RANS based CFD programs have become an accepted method of making predictions of flow patterns, pressures and the forces resulting from water flow around a ship's hull. The main advantages of using a commercial code are that the user interfaces are flexible and well designed and the codes are validated by a larger number of users in many fields of fluid dynamics and thermodynamics. The disadvantages are that they are very general in their application, and may be more complicated or less reliable to use than a custom made code for a very specific application.

The commercial RANS based CFD program used at Memorial University of Newfoundland is *Fluent* (Fluent Inc., 2005). Meshes for this program can be created in a number of different ways, but *Gambit* (Fluent Inc., 2005) is the product supplied by the same company for this purpose, and was the program used for this study.

Within *Gambit*, there are two distinct approaches for creating a mesh. The simplest type of mesh to generate is a tetrahedral mesh, where four points define individual cells and four triangular faces define a volume. This type of mesh can be generated very quickly using *Gambit*, once the basic size of the elements has been specified. The disadvantage of this approach is that the user has relatively little control over the size of the elements, beyond the definition of faces attached to boundaries within the mesh.

An alternative approach is to use a hexahedral mesh, where eight points and six faces define individual cells. When using *Gambit*, this type of mesh is much harder to define when boundaries of the cells must be fitted to the surface of the ship's hull. It requires the complete definition of the hull surface with four sided faces, and the definition of construction planes radiating out from the hull surface, which can also be defined by elements with four sided faces. The result is that the user has much more control over the definition of the mesh, but the time and effort required for this type of definition is much higher than that required for the tetrahedral mesh.

Gambit also has the capability to use a hybrid mesh, which is a combination of tetrahedral and hexahedral meshes within one continuous fluid volume. Since the main challenge found in conducting this study was accurate definition of the hexahedral mesh close to the hull, only two cases were considered, based on complete tetrahedral meshes or complete hexahedral meshes.

There are several trade-offs to be considered when developing the most appropriate mesh for a CFD prediction of the flow around a ship with a yaw angle. These are:

- 1) Accuracy of results
 - a) Hydrodynamics Forces
 - b) Flow patterns (including free surface waves)
- 2) Level of operator skill and time required for creating the mesh
- 3) Computer power required for solving the problem

The most effective way to evaluate the different meshing strategies was to compare the results of the CFD predictions against measured data for the same flow conditions. Comparing forces predicted by CFD programs against experiment data is relatively straight forward, but evaluation of the predicted flow patterns is more complicated. Most published research comparing CFD predictions of flow patterns with experiment results is done in a subjective way, and does not put numerical values on the comparison. A numerical index of the goodness of fit for the flow patterns is important in determining if one CFD model is better than another, but there does not appear to be an accepted method of doing this. A method was developed which allows numerical comparison of CFD predictions against measured data, and in turn, enables the selection of the method that gives the ‘best fit’ to observed flow patterns.

The main consideration for this research was the flow around a ship with a yaw angle, so it was important to obtain experiment results for this condition. In reviewing the available cases in the literature, two examples were found. Each case was for the Series 60 hull, with a block coefficient of 0.6 (Todd, 1963). Data was collected for a yaw angle of 10 degrees (Longo and Stern, 1996 and 2002) and a yaw angle of 35 degrees (Di Felice and Mauro, 1999). The bodyplan for this ship is shown in Figure 1. The hull has very fine waterlines in the bow and stern and a midship section with a relatively large bilge radius. A summary of the principal particulars is given in Table 1.

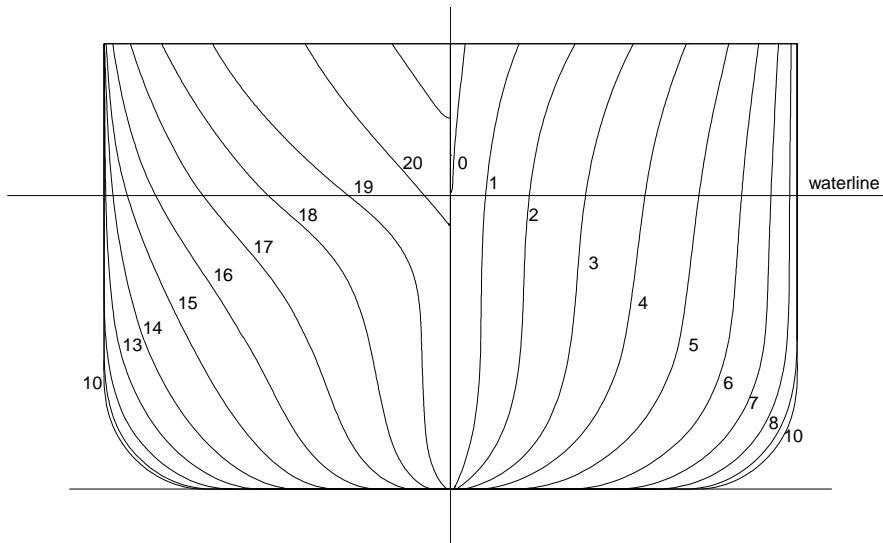


Figure 1, Series 60, $C_B=0.6$, Body plan for hull showing 21 equally spaced sections along waterline length

	Full scale	Iowa model (Longo & Stern, 1996, 2002))	INSEAN model (Di Felice & Mauro, 1999)
Length, BP, m	121.92	3.048	1.219
Beam, m	16.256	0.406	0.163
Draft, m	6.502	0.163	0.065
Wetted area, m ²	2526.4	1.579	0.253
C _B	0.6	0.6	0.6
C _M	0.977	0.977	0.977
Scale		1:40	1:100

Table 1, Principal Dimensions for Series 60, C_B=0.6

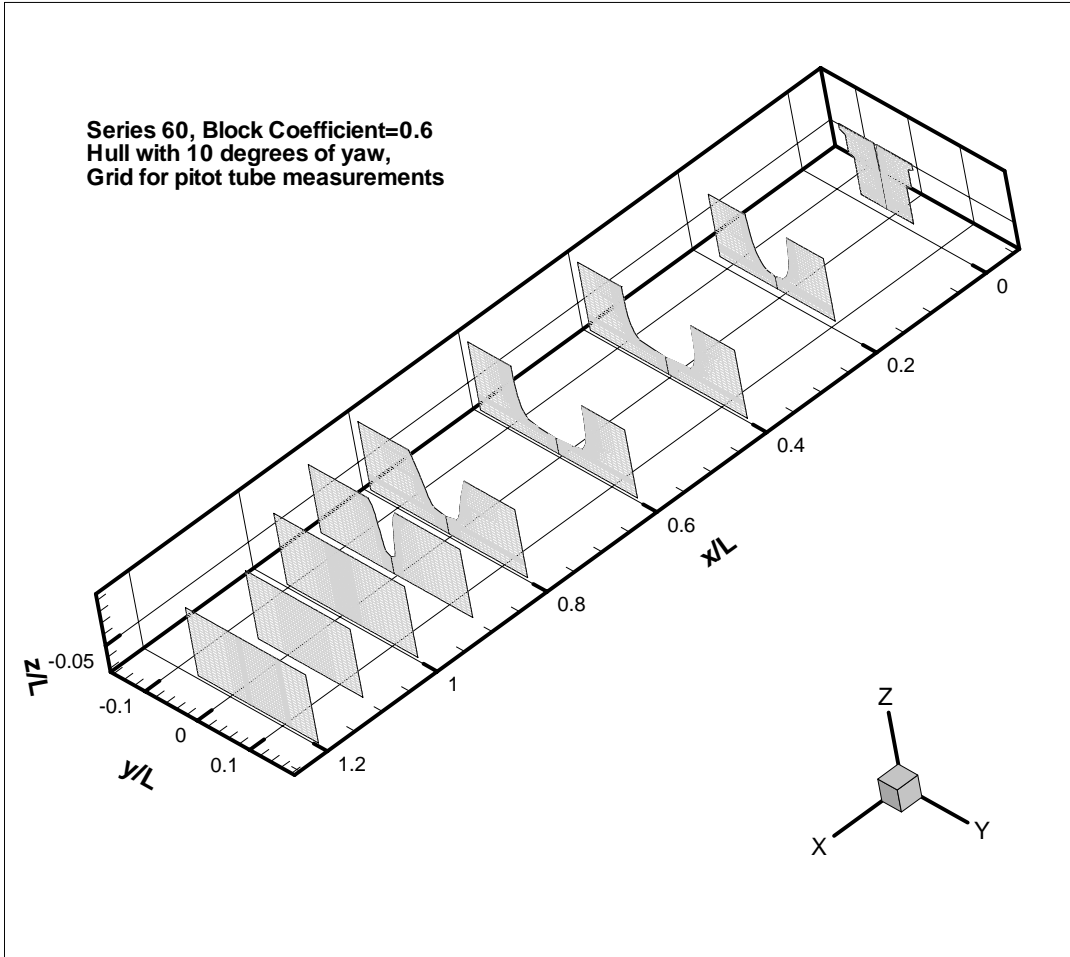


Figure 2, Measurement grid for Series 60, C_B=0.6 at 10 degrees yaw

DESCRIPTION OF SERIES 60 $C_B=0.6$ MODEL EXPERIMENTS

Pitot Tube Data for Yaw Angle of 10 Degrees

An extensive flow survey around a model of the Series 60, $C_B=0.6$ hull was made using five-hole pitot tubes for zero yaw angle (Toda et al., 1992, Longo et al., 1993) and with a 10 degree yaw angle (Longo and Stern, 1996, 2002). The experiments were carried out to determine the influence of waves created by a surface-piercing hull on its wake and boundary layer and to provide detailed measurements of the flow field for validating CFD methods. Mean velocity and pressure measurements were made for two Froude numbers (0.160 and 0.316) at multiple sections from the bow to the stern, and into the near wake at the stern. The two speeds were chosen to give the effects of waves on the flow.

A Cartesian measurement grid was used with the origin at the intersection of the forward perpendicular and the static waterline. The x -axis was positive towards the stern, the y -axis was positive to starboard and the z -axis was positive upwards. Velocities in the x , y and z direction were referred to as u , v and w respectively. Results were non-dimensionalized using model length (between perpendiculars) L , carriage velocity U and fluid density ρ . Two models were tested, at scales of 1:40 and 1:66.7.

Data from the experiments was presented as total pressure head and axial (u) velocity contours, cross plane (v , w) velocities and pressures and axial vorticity contours. The y - z planes were at locations of 0, 0.1, 0.2, 0.4, 0.6, 0.8, 0.9, 1.0, 1.1 and 1.2 L for each of the two Froude numbers. Wave profiles at the hull surface, contours of wave elevation and wave slope were also measured. Pressure measurements with the pitot tubes were made at between 200 and 350 locations per section.

Wave profiles at the hull were measured at more locations than the pressures. Wave elevation was measured using an array of wave probes fixed in the tank axis system, referred to in the paper as global elevations. Wave elevation close to the model was measured from a moving wave probe on the towing carriage, and this was referred to as local elevation. For the zero yaw case, the results presented were based on the combination of approximately 4000 carriage runs.

The work at 1:40 scale was expanded to include steady yaw angles up to 10 degrees (Longo & Stern, 1996, 2002). Forces and moments were measured for yaw angles from zero to 10 degrees at intervals of 2.5 degrees. Wave profiles at the hull surface and wave elevations were measured at yaw angles of zero, 5 and 10 degrees. Detailed pressure measurements were made at 10 degrees only. The methods used were essentially similar to the ones discussed above, with some minor changes. The biggest difference was that the range of the local wave surface measurements had to be extended, since the projected beam of the ship was wider, due to the yaw angle. Also, measurements were required on both sides of the hull, since the flow was no longer symmetric about the centerline.

The more complex flow around the yawed hull required a more precise spatial definition than the symmetric flow, and so data density for measurements was increased to between

800 and 1500 points per y - z plane. Data was collected for the upstream and downstream sides of the hull. The measurement grid for the case with 10 degrees yaw is given in Figure 2.

The results of the experiments for the zero yaw and the yawed case are available from the web site of the Computation Ship Hydrodynamics Laboratory at the University of Iowa (<http://www.ihr.uiowa.edu/~shiphydro/efd.htm>). For the purposes of this research, these data were re-plotted as contours of longitudinal flow velocity, u (non-dimensionalized by the free stream speed, U) and vectors of in-plane flow components (v - w , also non-dimensionalized by the free stream speed, U) for selected sections along the hull.

For evaluation of the CFD predictions, only three of the sections were chosen. These were $20\%L$, $60\%L$ and $90\%L$ aft of the fore perpendicular. The data from Longo and Stern for these sections are shown plotted in Figures 3 to 5. These sections were picked because they showed the development of a vortex within the flow, and this vortex moved, relative to the centreline of the ship, as the section location was changed. It was important for the CFD code to be able to predict these flow patterns.

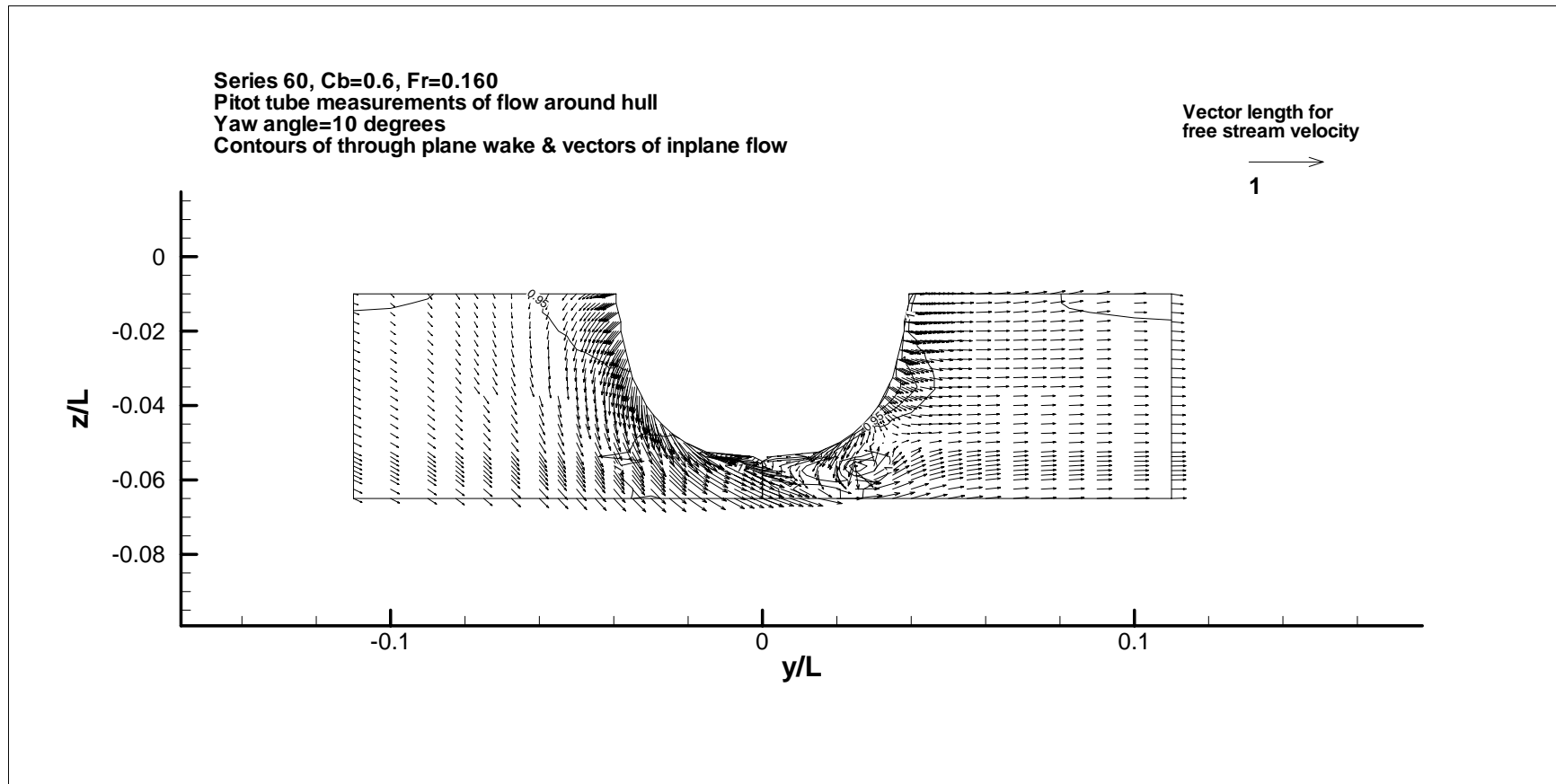


Figure 3, Results of pitot tube survey for flow around Series 60, $C_B=0.6$, section at $20\%L$

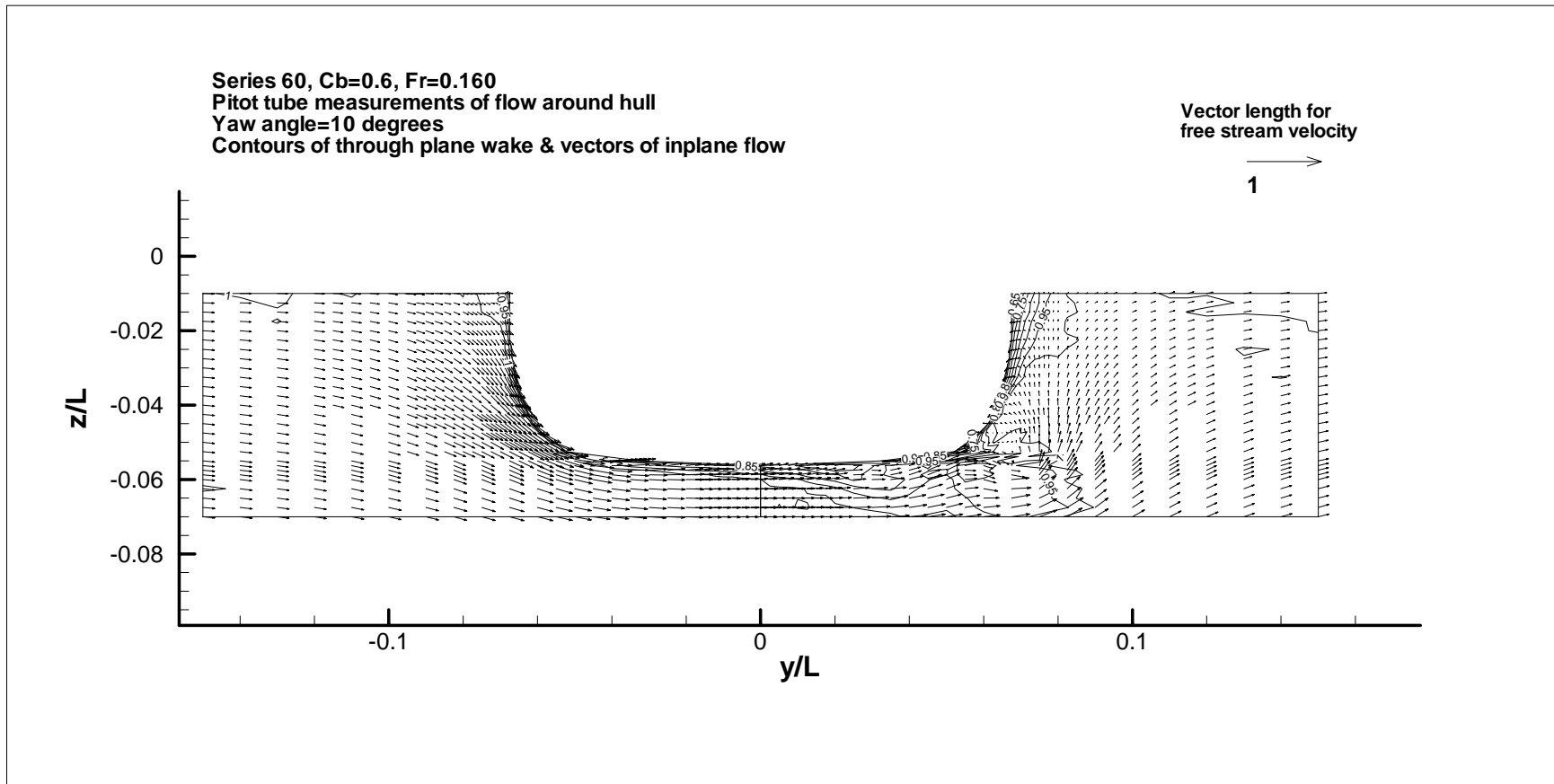


Figure 4, Results of pitot tube survey for flow around Series 60, $C_B=0.6$, section at 60% L

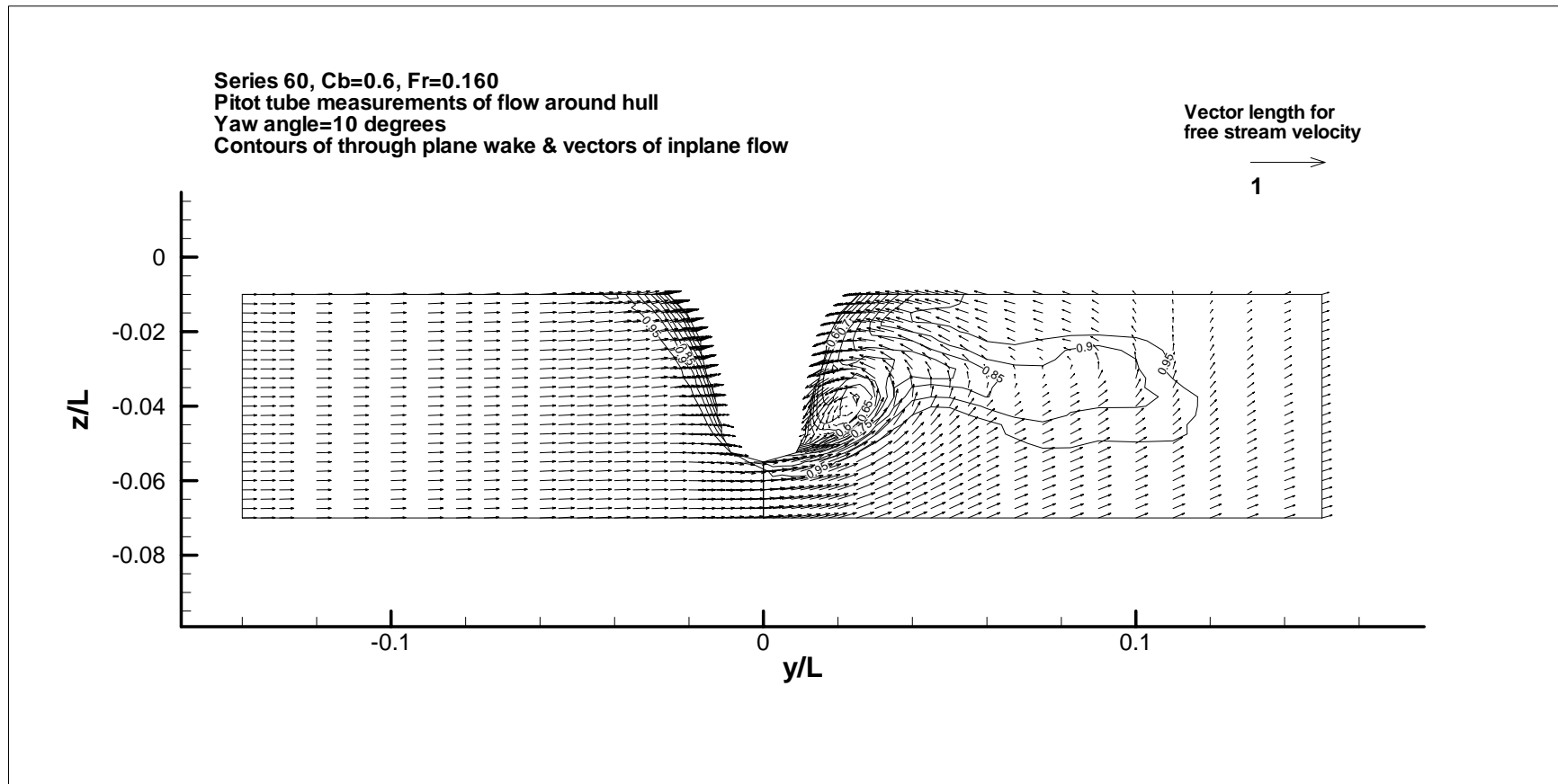


Figure 5, Results of pitot tube survey for flow around Series 60, $C_B=0.6$, section at 90%L

All these figures are for a Froude number of 0.16. The results for Froude number of 0.316 showed similar flow patterns. The Froude number of 0.16 was chosen because it was within the expected Froude number range for escort tugs, and was a close match to the speed used by Di Felice and Mauro (1999) for their experiments, which are discussed below.

LDV Data for Yaw Angle 35 Degrees

Di Felice & Mauro (1999) measured the flow on the downstream side of a double model of a Series 60 $C_B=0.6$ hull at a scale of 1:100 in a large cavitation tunnel using Laser Doppler Velocimetry (LDV). In this case, the model hull was symmetrical about the design waterline and the free surface effects were ignored. The yaw angle used was 35 degrees, which is within the expected range of operating yaw angles for an escort tug. The Froude number used for these experiments was 0.2, although the free surface was not considered. The flow speed for these experiments was 0.692 m/s.

The LDV used a two-component backscatter method, with estimated velocity resolutions within +/-1%. The flow was seeded with titanium dioxide particles, with a diameter of 1 μm . Measurements were made at two sections, $0.5L$ and $0.9L$. The data density was 600 points for the first section and 800 points for the second. The measurements were made in the axis system of the tunnel, rather than normal to the centerline of the model. The resulting measurement planes were not at a constant location in ship axes, which was the convention used by Toda et al. (1992) and Longo and Stern (1996, 2002). They were normal to the direction of the undisturbed flow, rather than normal to the centreline of the ship. This was accepted in order to use the mechanized system for locating the measurement point within the flow, which was fixed in an axis system with the y and z -axes normal to the centerline of the cavitation tunnel. Also, the origin for the system was at the aft perpendicular for the model.

The data from the two yaw angles were obtained in two different axis systems. Each system was chosen for valid reasons based on the nature of the experiments and the facility in which the experiments were carried out. Longo and Stern chose a ship based axis system for measurements in a towing tank. In this system, all measurements were made relative to an axis based on ship coordinates. The three orthogonal axes were defined relative to the centreline of the ship and undisturbed flow crosses the measurement plane at an angle. Di Felice and Mauro chose a measurement axis system based on the flow direction, since they did their experiments in a cavitation tunnel with the measurement system fixed in a direction normal to the centreline of the tunnel. The resulting measurement plane was normal to the undisturbed flow direction. The two axis systems are illustrated for the Series 60 hull at $50\%L$ and $90\%L$ for 35 degrees of yaw in Figure 6.

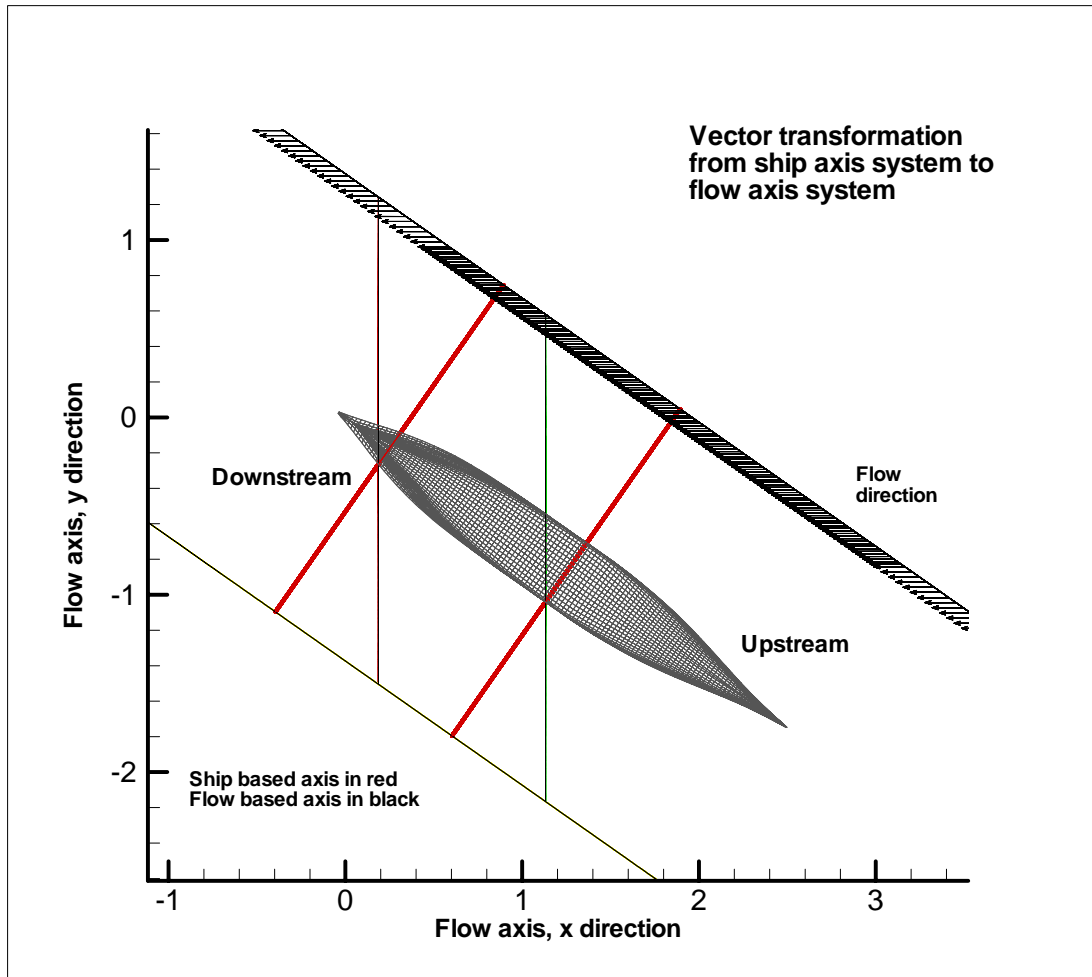


Figure 6, Measurement planes for Series 60, $C_B=0.6$ at 35 degrees of yaw,
Ship based coordinates in red, flow based coordinates in black

Measured flow vectors in the two planes are shown in Figure 7 and 8. Both planes are on the downstream side of the model. The geometric locations were non-dimensionalized by ship length and the mean flow speeds were non-dimensionalized by the speed of the undisturbed flow.

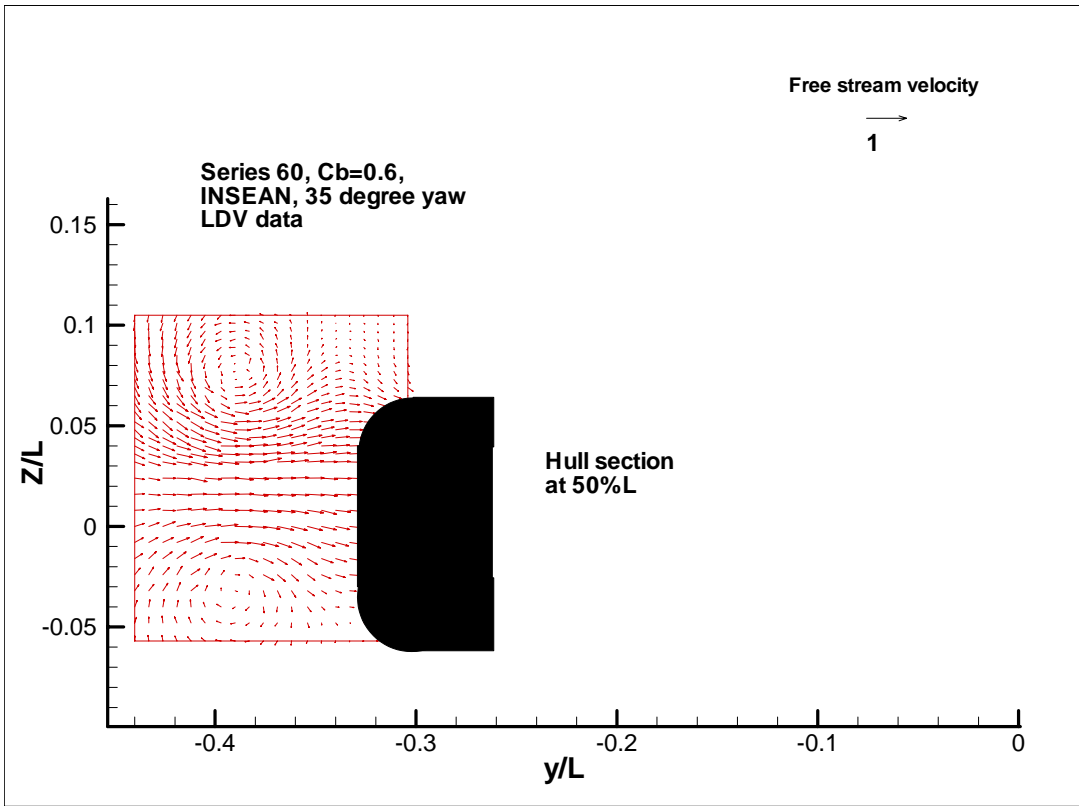


Figure 7, Flow vectors measured at 50%L, 35 degrees of yaw

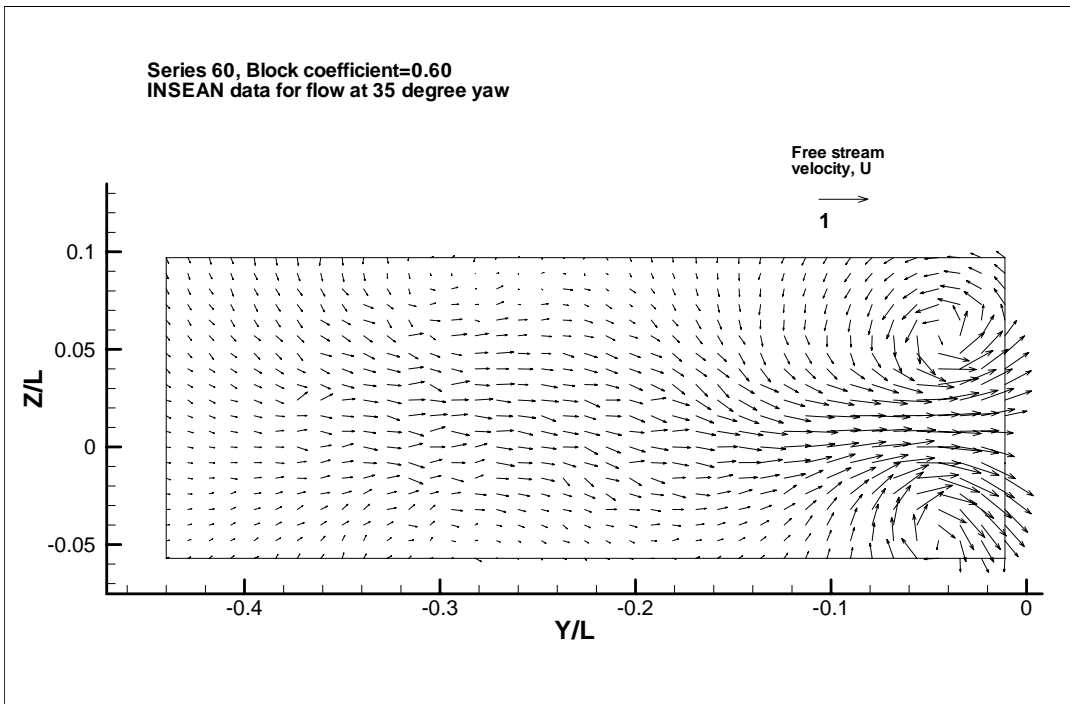


Figure 8, Flow vectors measured at 90%L, 35 degrees of yaw

Since the model was symmetrical about the waterline, the results shown in Figures 7 and 8 should be symmetrical about the z/L value of zero, and this is the case, within an allowance for scatter in the results of the experiments (although it looks as though the model may have had a small pitch angle, since the two vortices in Figure 7 are not at the same z/L location).

Based on the geometry of the experiment, the maximum beam of the hull at $50\%L$ was at a value of y/L approximately -0.34 and the maximum draft was at z/L of ± 0.059 . Figure 7 shows the approximate locations of the maximum beam and maximum draft within the measurement coordinate system. Note that the origin used in these experiments was at the aft perpendicular and fixed in the axis of the cavitation tunnel, rather than the ship.

Results of the experiments were presented by Di Felice and Mauro (1999) as contours of cross flow velocities, vertical and transversal component standard deviation, Reynolds stresses, vorticity and vertical and transverse component skewness for the downstream side of the hull. The results showed distinct vortices at each plane. Di Felice and Mauro state that the advantage of the LDV method was the ability to measure quantities such as turbulence intensity and Reynolds stresses, as well as detailed measurements of the flow in the cross planes. All these results combined to give information on viscous and turbulent aspects of detached flow generated by the yawed hull.

The data from the experiments was faired by assuming that the lower portion of the measurements was a mirror of the upper. The z/L value used for folding the data was not the same for each case. For $50\%L$ the fold was at $z/L=0.016$, and for $90\%L$, the fold was at $z/L=0.008$. These values were chosen to make the centre of the observed vortex symmetrical about the nominal waterline of the model. Average values for the vectors were used, based on the measured values for the upper and lower sections of the hull. Measured data points that were inside the model geometry or very close to the surface of the hull were removed before the results were compared to the CFD predictions.

MESHING STRATEGIES FOR HULLS WITH YAW

Previous CFD Solutions for Flow Around Series 60 $C_B=0.6$ Hull

The experiment data for the Series 60 $C_B=0.6$ hull with a yaw angle of 10 degrees were compared with numerical predictions for the same conditions by Alessandri and Delhommeau (1996), Cura Hochbaum (1996), Campana et al. (1998) and Tahara et al. (2002). All of the methods solve the RANS equations for turbulent flow with a free surface but each author used a different turbulence model. In each case, the computational grid conformed to the body surface and the free surface, using hexahedral grid elements. Predictions were made for Froude numbers of zero (no free surface) and 0.316. All of the authors claim that their method captured the essential features of the flow, such as the asymmetric wave field close to the hull, mean flow fields dominated by strong cross flow effects and asymmetric vorticity distributions along the hull. However, in all cases the agreement was discussed subjectively, without putting any numerical values on the level of accuracy.

The use of hexahedral elements in the computational grid is widely accepted for CFD calculations of flow around ships. One exception to that is the code *FEFLO* (Yang and Löhner, (1998), Löhner et al., (1999)), which only uses a tetrahedral mesh. It was discussions with Professors Löhner and Yang during a visit to St. John's in September 2005 that initiated the consideration of a fully tetrahedral mesh as a suitable solution for a ship hull with a yaw angle.

Mesh Development

In practical situations, high yaw angles for ships only occur at low Froude numbers, where wave making generally has a small effect. At high speeds and high yaw angles, the side force components are large relative to the forward force components and act to slow down the ship. The large forces also generate large heeling and yawing moments. As a result, it is possible to ignore the free surface for ships with large yaw angles, since practical applications will result in a Froude number based on ship length of under 0.2.

The results of the experiments from Di Felice and Mauro (1999) did not consider a free surface. Results of the flow measurements at 10 degrees of yaw were available for two Froude numbers ($Fr=0.16$ and 0.32), but for this study, only the lower one was considered. To simplify the meshes developed for this study the free surface was ignored. This was primarily because the main objective of this study was to evaluate the effectiveness of the different mesh strategies, at low Froude numbers, and so ignoring the free surface effects should only have a small effect on the results.

Each mesh strategy was subject to a certain amount of trial and error to obtain acceptable results, which was not described here. For the tetrahedral mesh this included experimentation with cell size and distances between the inner and outer mesh. For the hexahedral mesh it included a sensitivity study (focusing on the thickness of the elements

close to the hull). Neither mesh strategy was the subject of a rigorous analysis of the effect of cell size and the proximity of the boundary conditions to the hull. The selection of the meshes used was based on a subjective comparison of the forces and flow patterns predicted by the CFD program.

Tetrahedral Mesh for Series 60 $C_B=0.6$

A file describing the hull surface for the Series 60 $C_B=0.6$ had been previously used at IOT for construction of a 1:20 scale model. This file was used as the starting point for generating the mesh within *GAMBIT*. This definition of the hull had the origin at the aft perpendicular, and was dimensioned in metres for the full-scale ship. The original hull surfaces were trimmed to the static waterline prior to meshing. The surfaces were then imported into *GAMBIT* as virtual surfaces. Small edges were removed and any edges of adjoining surfaces that did not match were connected. Also some surfaces defined in the original geometry were merged to make the meshing easier.

The next step was to create the domain boundaries and any additional surfaces required for constructing the mesh. For the tetrahedral mesh, three basic volumes were used within the overall geometry. The smallest volume was close to the hull and contained the smallest elements. These were uniform sized elements with a nominal dimension of 1 metre. Two additional volumes were defined. The outer volume included the domain boundaries, and this was meshed with elements with a nominal dimension of 10 metres at the outer boundary, but reduced in size closer to the hull. A third volume between the inner volume and the outer volume was required to provide a transition region between the two. The geometry of each region is given in Table 2. An overview of the complete mesh is shown in Figure 9. Key sections along the hull are shown in Figure 10, for the region close to the hull. This is the region in which measurements were made during the experiments. The mesh shown has been converted to the same coordinates used in the experiments at 10 degrees of yaw (Longo and Stern, 1996).

Volume	Element size, m	X, min, m	X, max, m	Y, min, m	Y, max, m	Z, min, m	Z, max, m
Inner	1	-5.0	130.0	-9.0	9.0	-0.498	6.502
Intermediate	Transition	-80.0	200.0	-20.0	20.0	-5.498	6.502
Outer	10	-200.0	200.0	-60.0	60.0	-23.498	6.502

Table 2, Summary of geometry, tetrahedral mesh

The total number of elements within the mesh was 1,759,560. The mesh was nominally symmetrical about the centreline.

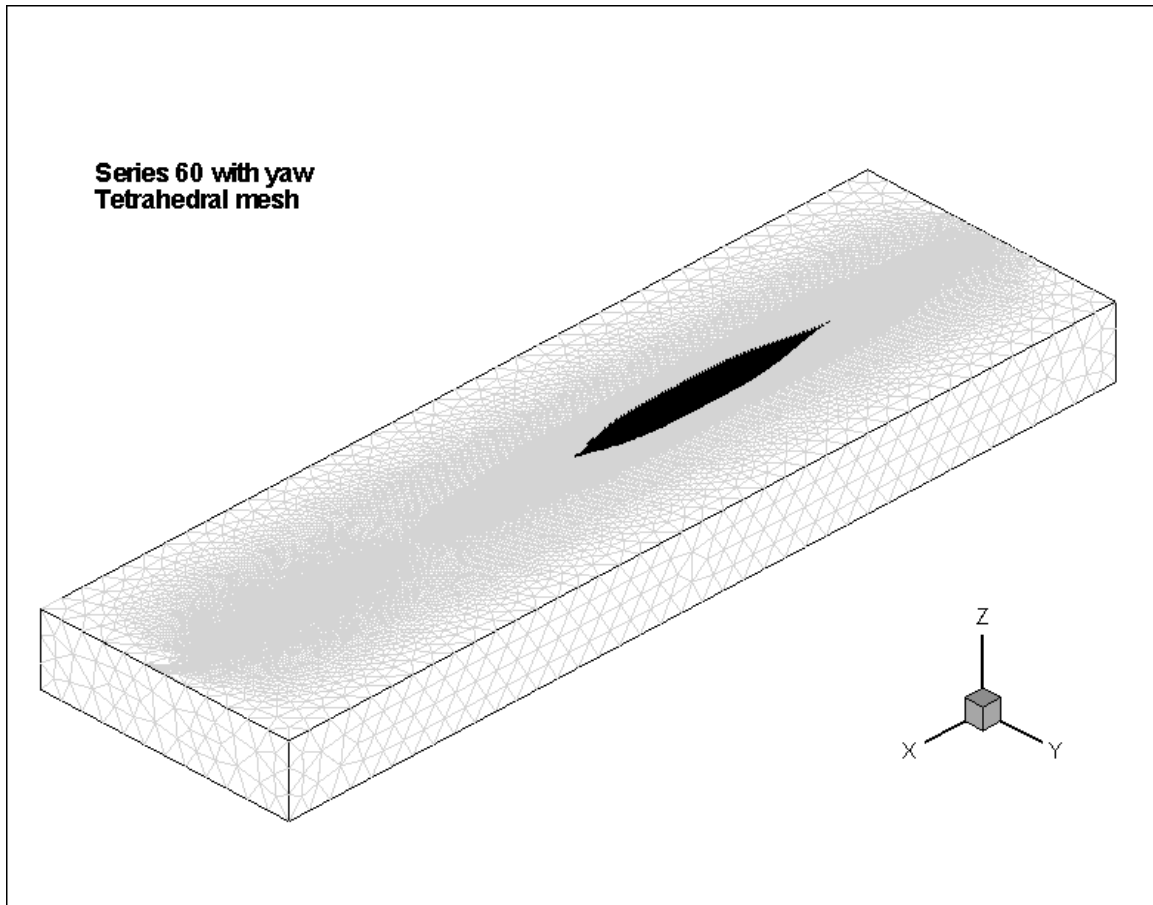
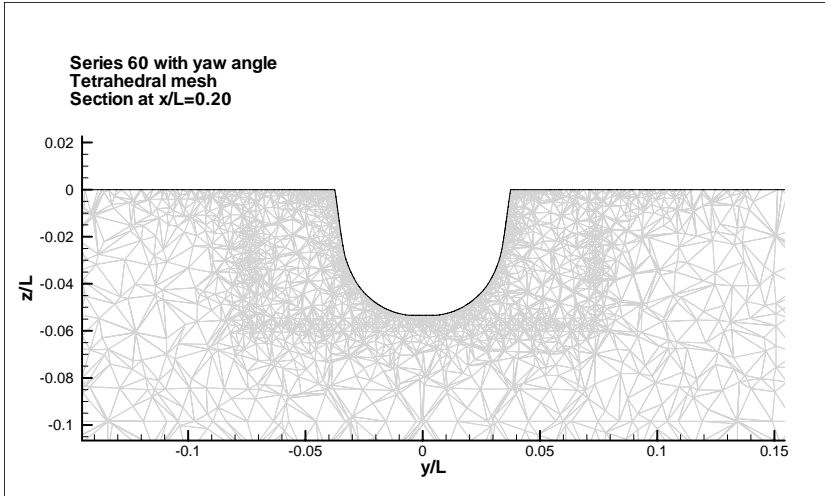
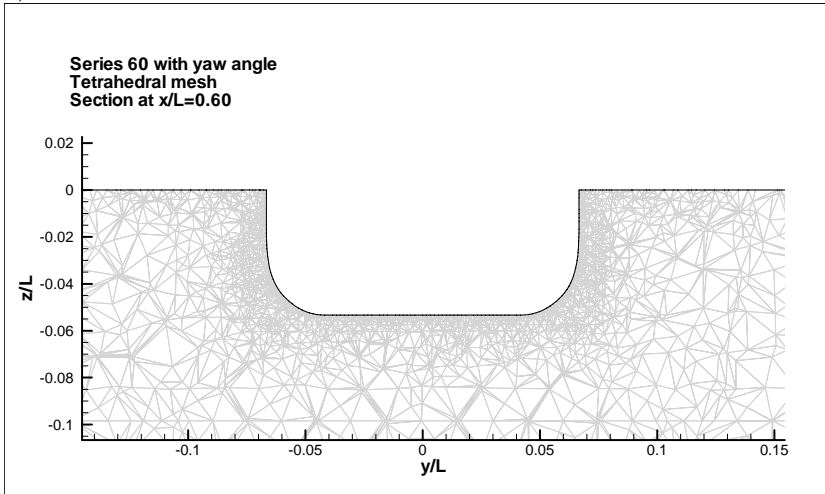


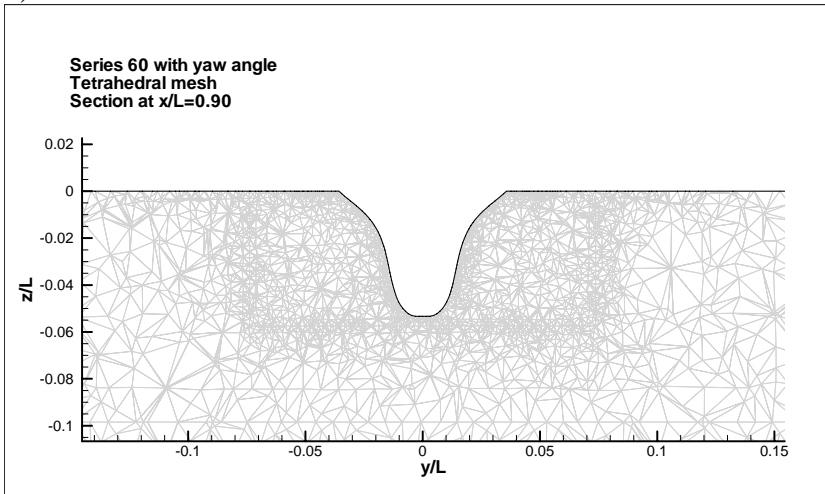
Figure 9, Overview of tetrahedral mesh, origin at bow, x positive towards stern



a)



b)



c)

Figure 10, Tetrahedral mesh at three representative sections

a) $0.20L$, b) $0.60L$, c) $0.90L$

Hexahedral Mesh for Series 60 $C_B=0.6$

The same surface file was used to create the hexahedral mesh as was used for the tetrahedral mesh. In this case the additional step of creating new surfaces so that the hull could be defined completely in four-sided elements was required. This was done within *Gambit*.

Again the mesh was divided into two regions. One region was close to the hull surface, and one was sufficiently far from the hull surface, that flow conditions were not changing significantly. The hull was defined using 16 cells from the centreline to the waterline, and this had to be kept constant along the whole length of the hull. This required a much more elaborate system of construction planes along the length of the hull, especially close to the bow and the stern.

Once the inner mesh was successfully defined, the cells in the y - z plane were extruded to the inlet and outlet boundaries. The mesh was symmetrical about the centreline of the ship.

A summary of the mesh geometry is given in Table 3.

Volume	X, min, m	X, max, m	Y, min, m	Y, max, m	Z, min, m	Z, max, m
Inner	-2.86	123.00	-15.0	15.0	-5.498	6.502
Outer	-127.86	185.50	-45.0	45.0	-23.498	6.502

Table 3, Summary of geometry, tetrahedral mesh

The total number of elements within the mesh was 423,464, which was less than one quarter of the number used for the tetrahedral mesh.

An overview of the complete hexahedral mesh is shown in Figure 11. Key sections along the hull are shown in Figure 12, for the region close to the hull, over which measurements were made during the experiments. The mesh shown has been converted to the same coordinates used in the experiments at 10 degrees of yaw described by Longo and Stern (1996, 2002).

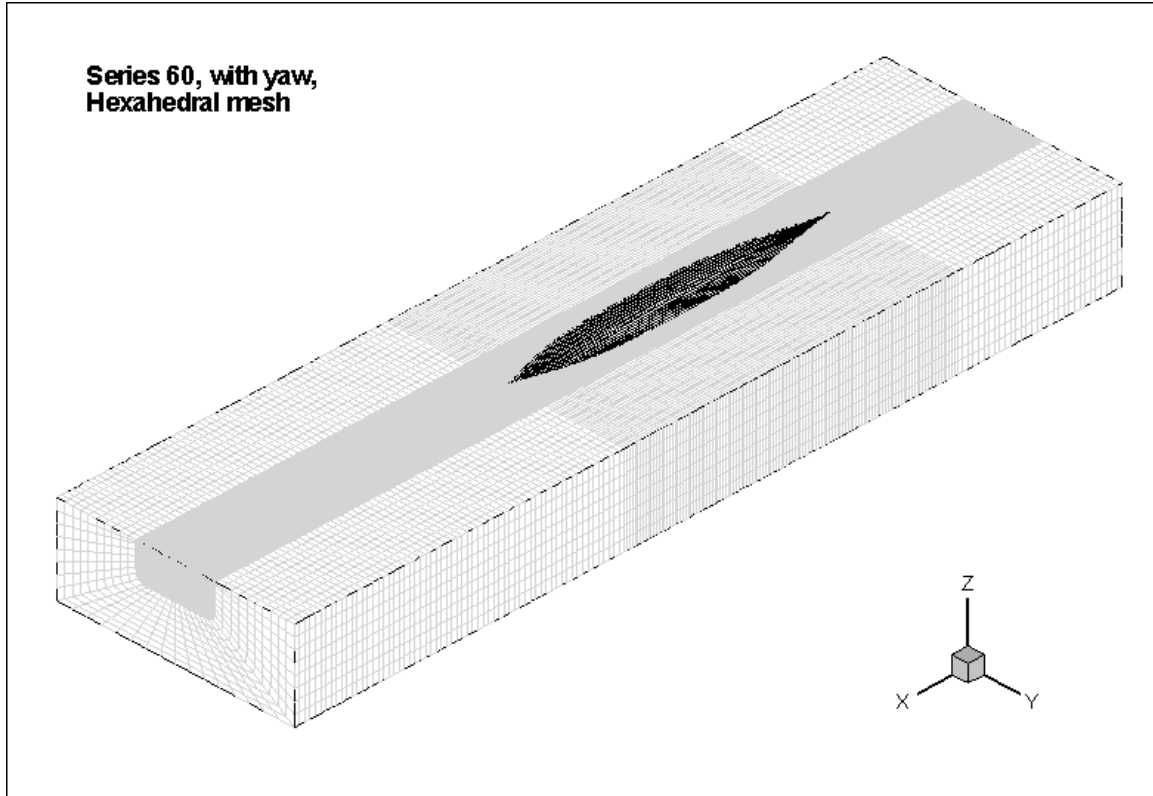
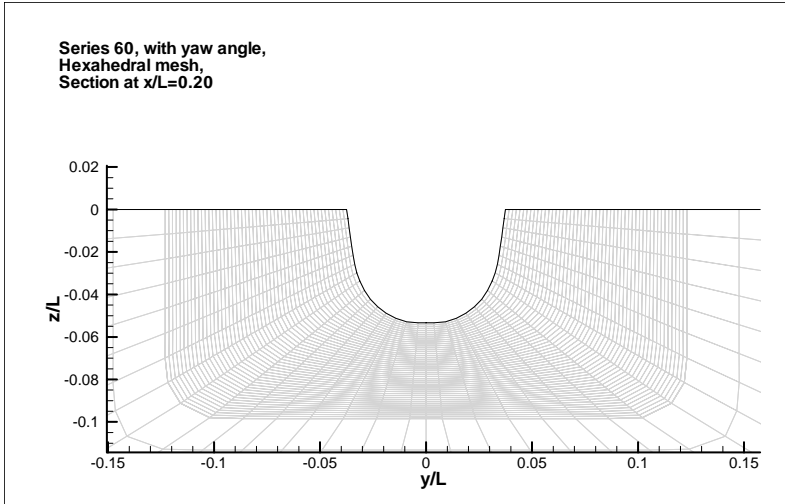


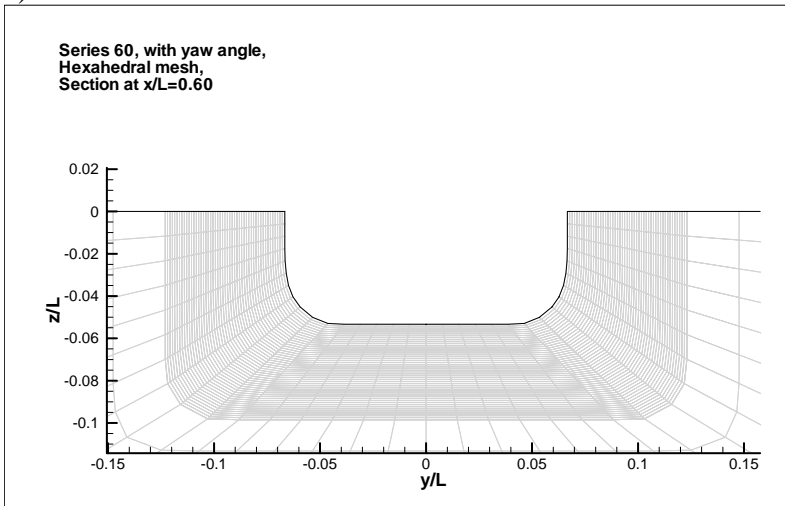
Figure 11, Overview of hexahedral mesh, origin at bow, x positive towards stern

α_{∞}^*	1.0
α_{∞}	0.52
α_0	0.111
β_{∞}^*	0.09
β_i	0.072
R_{β}	8
ζ^*	1.5
M_{t0}	0.25
TKE Prandl number	2
SDR Prandl number	2

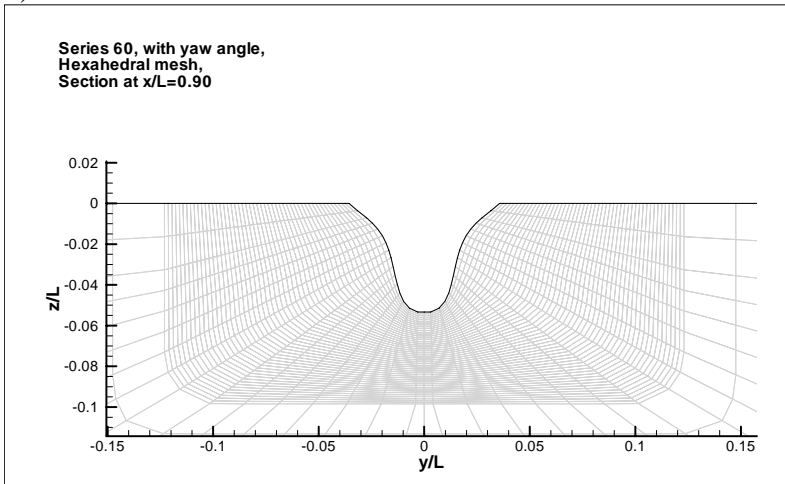
Table 4, Parameters for κ - ω turbulence model



a)



b)



c)

Figure 12, Hexahedral mesh at three representative sections
a) $0.20L$, b) $0.60L$, c) $0.90L$

CFD Solutions Obtained Using *Fluent*

The upstream end and upstream side of the domain were defined as velocity inlets and the downstream end and downstream side were defined as pressure outlets. The hull was defined as a no-slip wall, and the upper and lower surfaces were defined as walls with zero shear force.

For the yaw angle of 10 degrees, the mesh coordinates were transformed within *Fluent*. The origin was moved to the fore perpendicular, and the x direction reversed so that it was positive towards the stern, and the y direction was also reversed. All values for the mesh were scaled down to represent a model at a scale of 1:40 and a flow speed of 0.875 m/s. Planes within the solutions at constant values of x/L (0.2, 0.6 and 0.9) were extracted for comparison with the results of the experiments. For the yaw angle of 35 degrees, the original coordinate system of the mesh was used, but additional planes were added to intersect the hull, on the downstream side at $50\%L$ and $90\%L$, which were normal to the undisturbed flow direction.

Predictions of the flow were obtained using *Fluent*. Boundary conditions, turbulence models and solution parameters for both the tetrahedral and hexahedral meshes were the same. Uniform flow entered the domain through a velocity inlet on the upstream boundaries and exited through a pressure outlet on the downstream boundaries. Yaw angle was changed by varying the direction of the flow vector at the boundary using a cosine component for flow along the centreline and a sine component for flow normal to the centreline on the inlet and outlet.

The selection of the turbulence model was based on discussions with experienced users of *Fluent* and other CFD codes (Rhee 2005, Turnock, 2006,). The turbulence model used within *Fluent* was the standard κ - ω model with shear force corrections, and the default parameters given in Table 4. This is an empirical turbulence model, based on model transport equations for the turbulence kinetic energy (κ) and the specific dissipation rate (ω). Turbulence intensity and turbulent viscosity ratios at the boundaries were set at 1% and 1 respectively. The flow was solved for the steady state case. The convergence limit was set to 10^{-3} (default values within *Fluent*) for all parameters. All solutions converged within these limits. Flow speeds were non-dimensionalized using the free stream flow speed for presentation of the results.

For the 10 degree yaw case, results of the tetrahedral mesh are shown in Figures 13 to 15, and for the hexahedral mesh in Figures 16 to 18. These predictions are for the same flow conditions as the experiments of Longo and Stern (1996, 2002) shown in Figures 3 to 5.

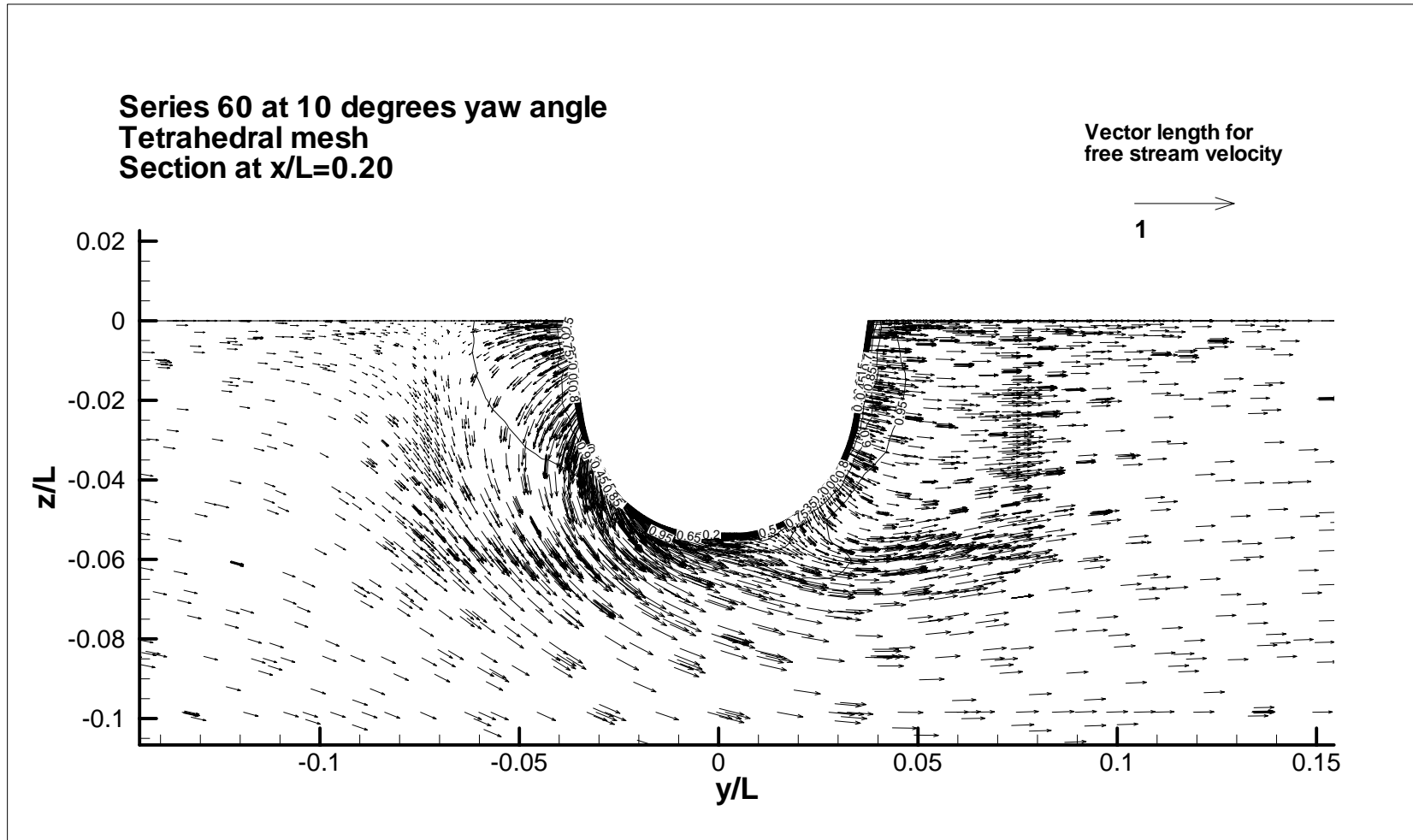


Figure 13, Tetrahedral mesh, Yaw angle 10 degrees, CFD predictions of flow patterns at $x/L=0.20$

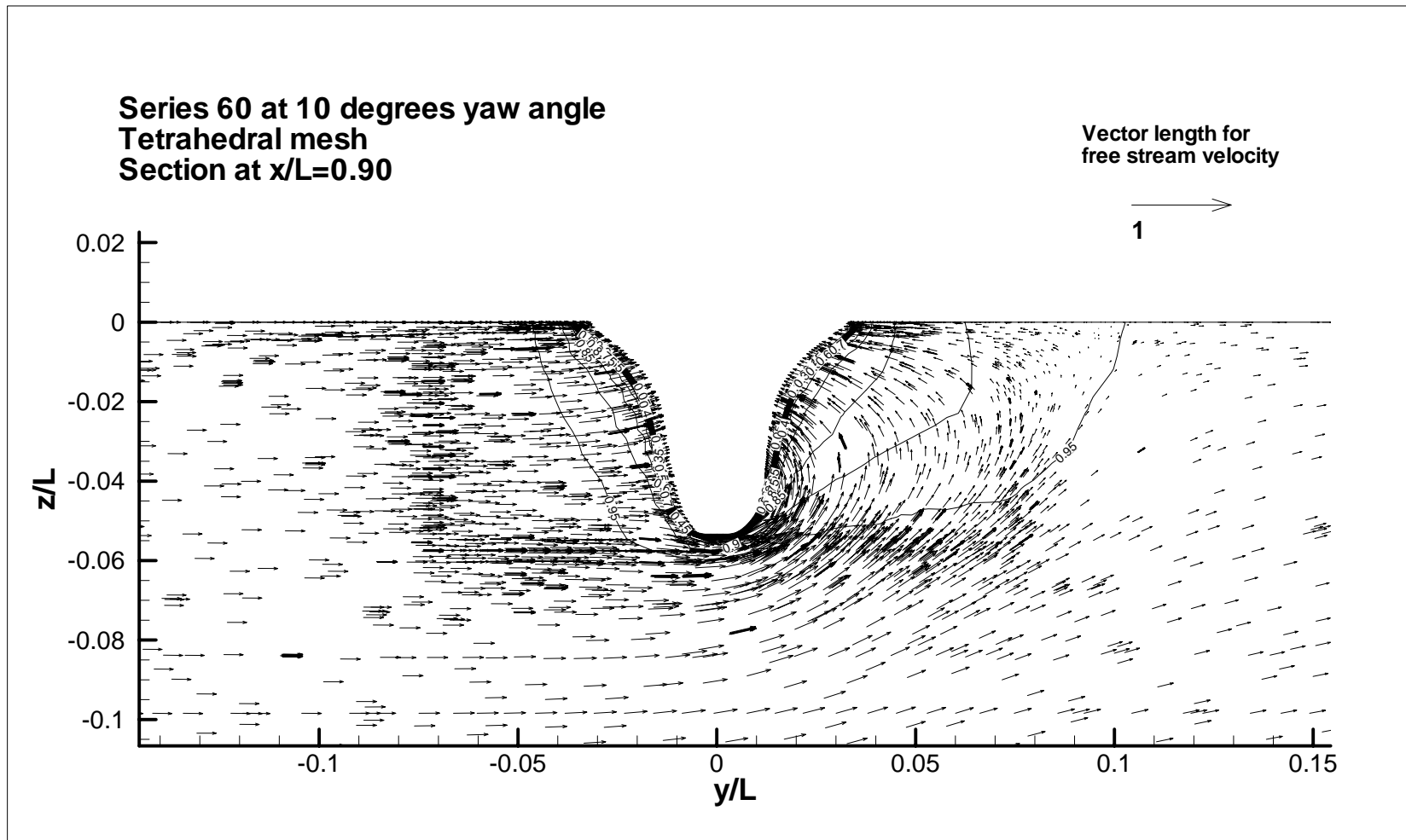


Figure 15, Tetrahedral mesh, Yaw angle 10 degrees, CFD predictions of flow patterns at $x/L=0.90$

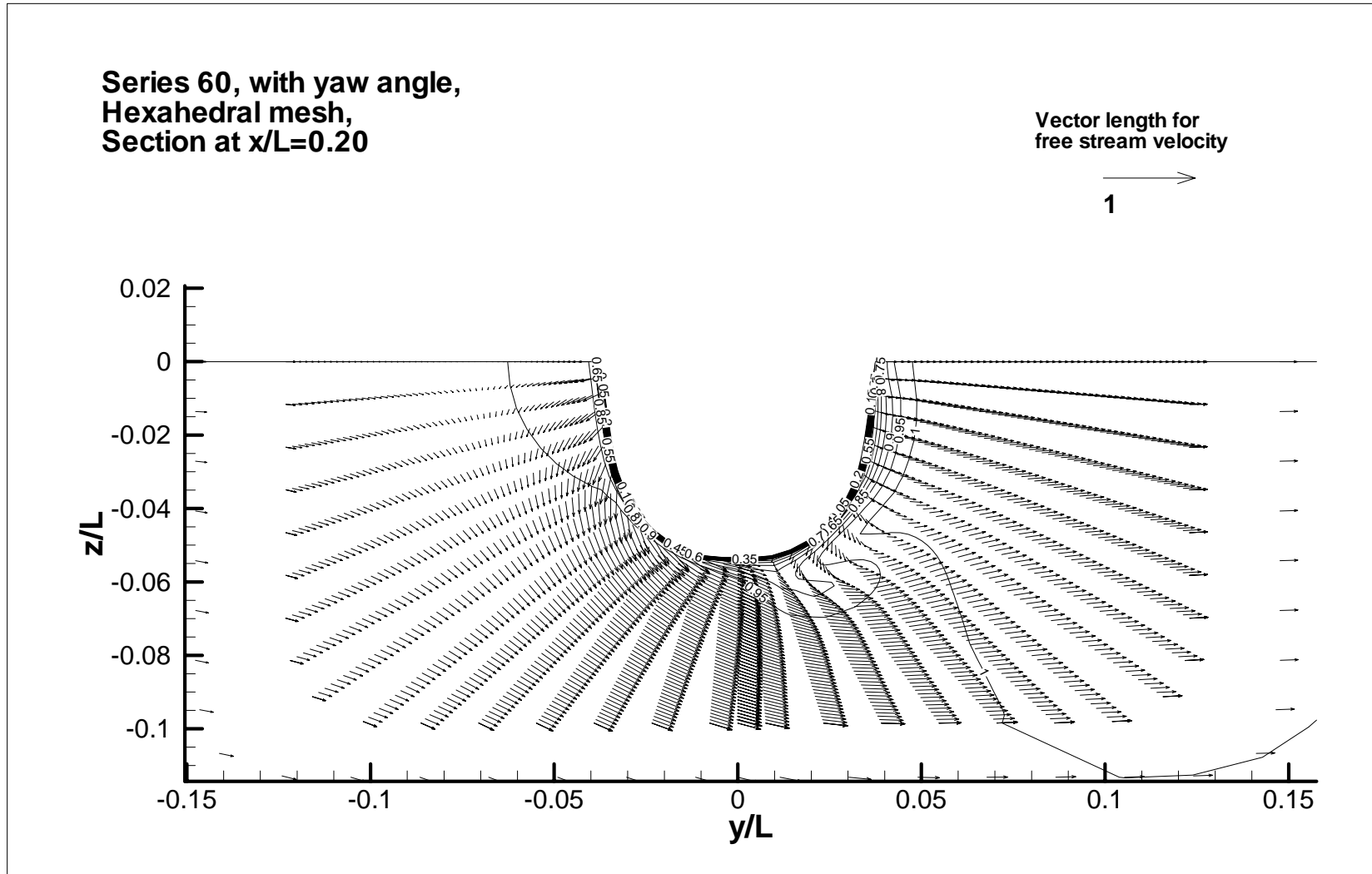


Figure 16, Hexahedral mesh, Yaw angle 10 degrees, CFD predictions of flow patterns at $x/L=0.20$

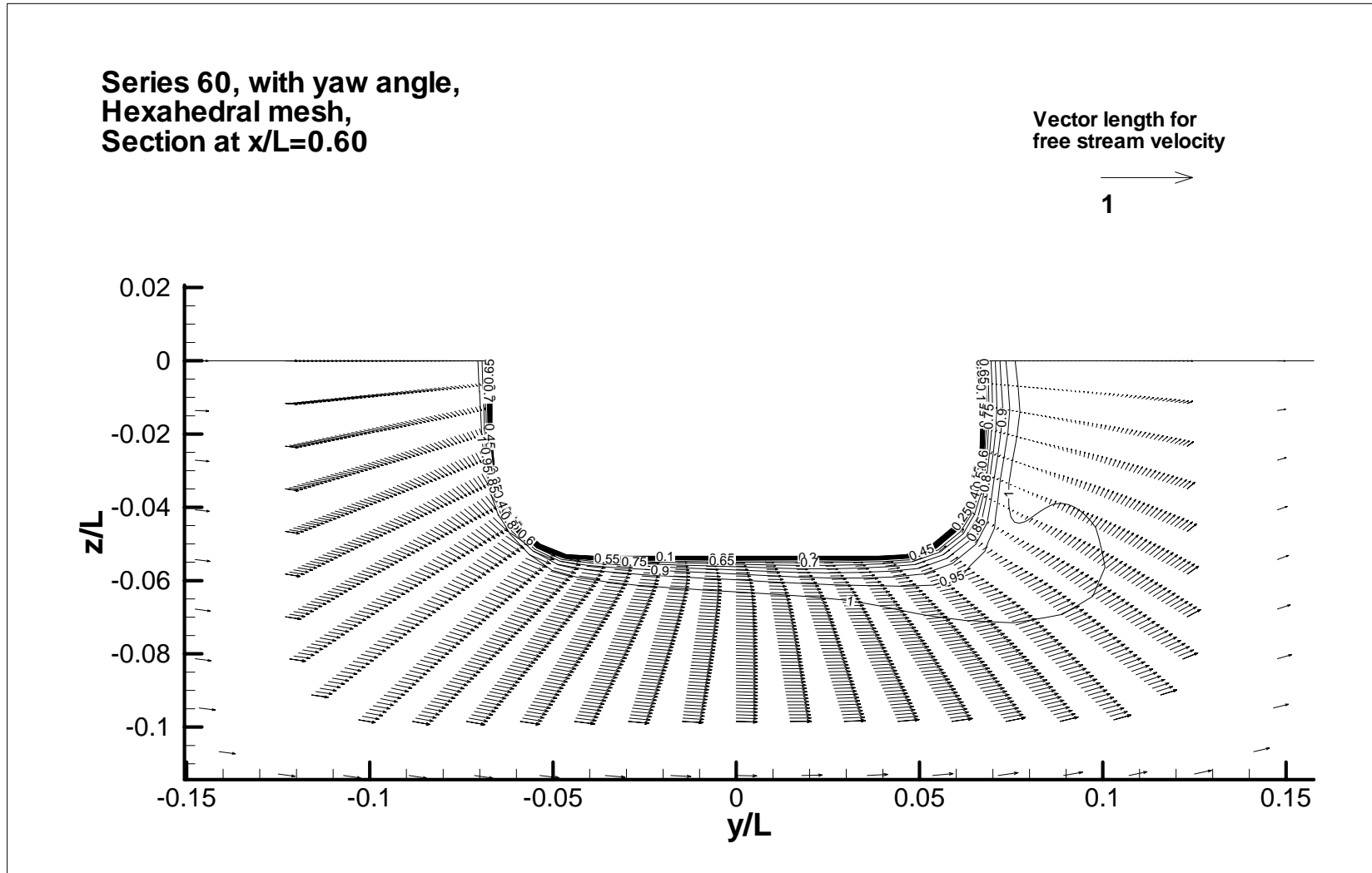


Figure 17, Hexahedral mesh, Yaw angle 10 degrees, CFD predictions of flow patterns at $x/L=0.60$

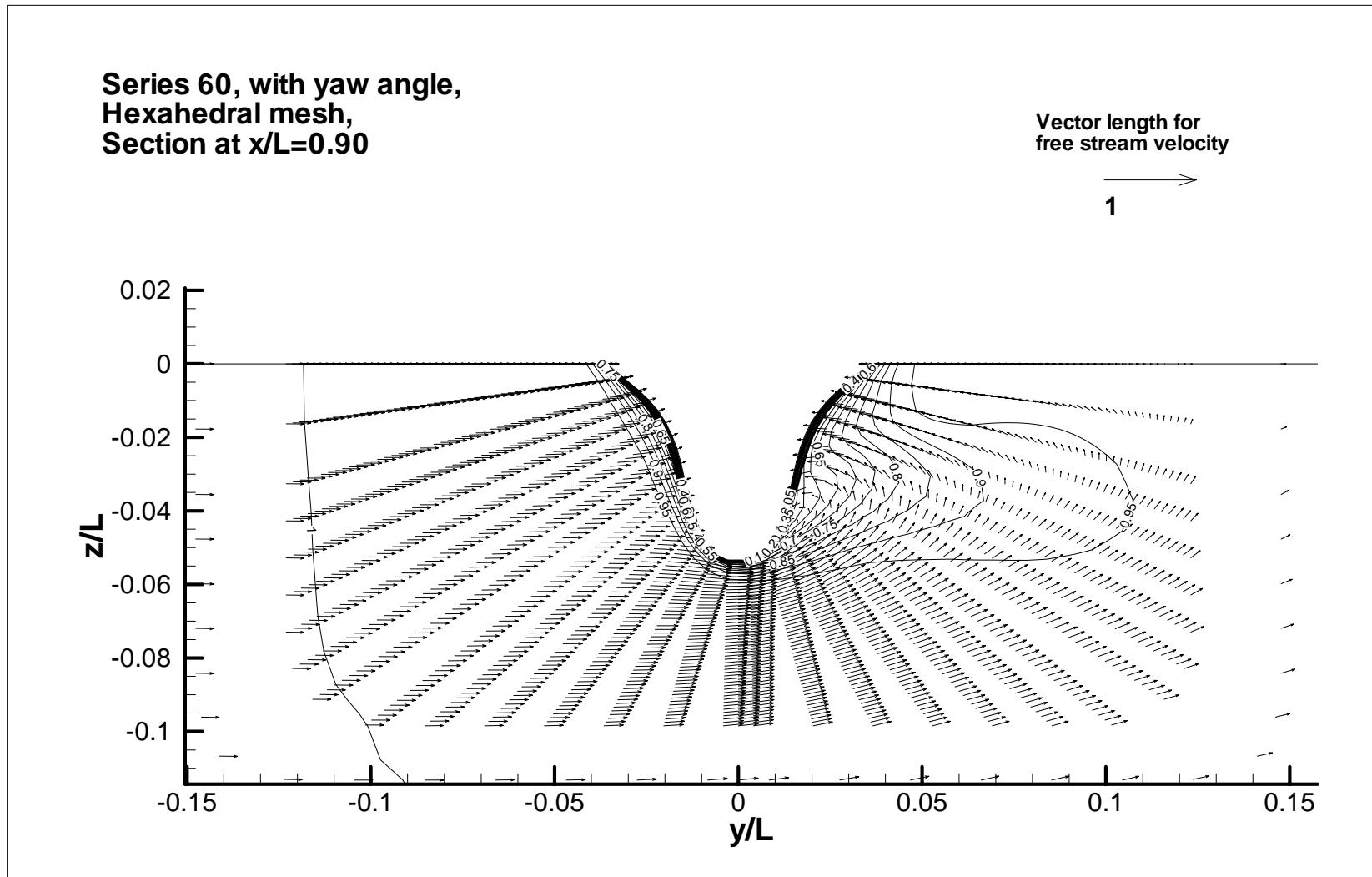


Figure 18, Hexahedral mesh, Yaw angle 10 degrees, CFD predictions of flow patterns at $x/L=0.90$

For comparing the CFD predictions with model experiments at 35 degrees of yaw, additional planes were created within the CFD solution, based on the measurement planes used in the experiments. The velocity components in these planes were given by *Fluent* in the original (ship-based) grid axis system. The results of the CFD simulations required some manipulation before they were comparable with the measurements made in the experiments. For the experiments at 35 degrees yaw, the origin was at the aft perpendicular of the model, with x direction positive towards the bow, and the flow components were in the negative x and y directions. The flow vectors and associated grid points taken from the CFD solution within the measurement planes were transformed into an in-plane and through-plane coordinate system using the following transformations;

$$x_f = (x_s \cos \theta + y_s \sin \theta)$$

$$y_f = (-x_s \sin \theta + y_s \cos \theta)$$

where;

x_f and y_f are in the flow based coordinates

x_s and y_s are in the ship based coordinates

θ is the angle between the flow direction and the ship based coordinates.

Since the transformation about the vertical axis was purely rotation, the third axis (z in the experiment notation) was unchanged.

The predicted flow patterns in the flow based axis system are shown in Figures 19 and 20 for the tetrahedral mesh and Figures 21 and 22 for the hexahedral mesh. These predictions can be compared to the results of the experiments given by Di Felice and Mauro (1999), shown in Figures 7 and 8.

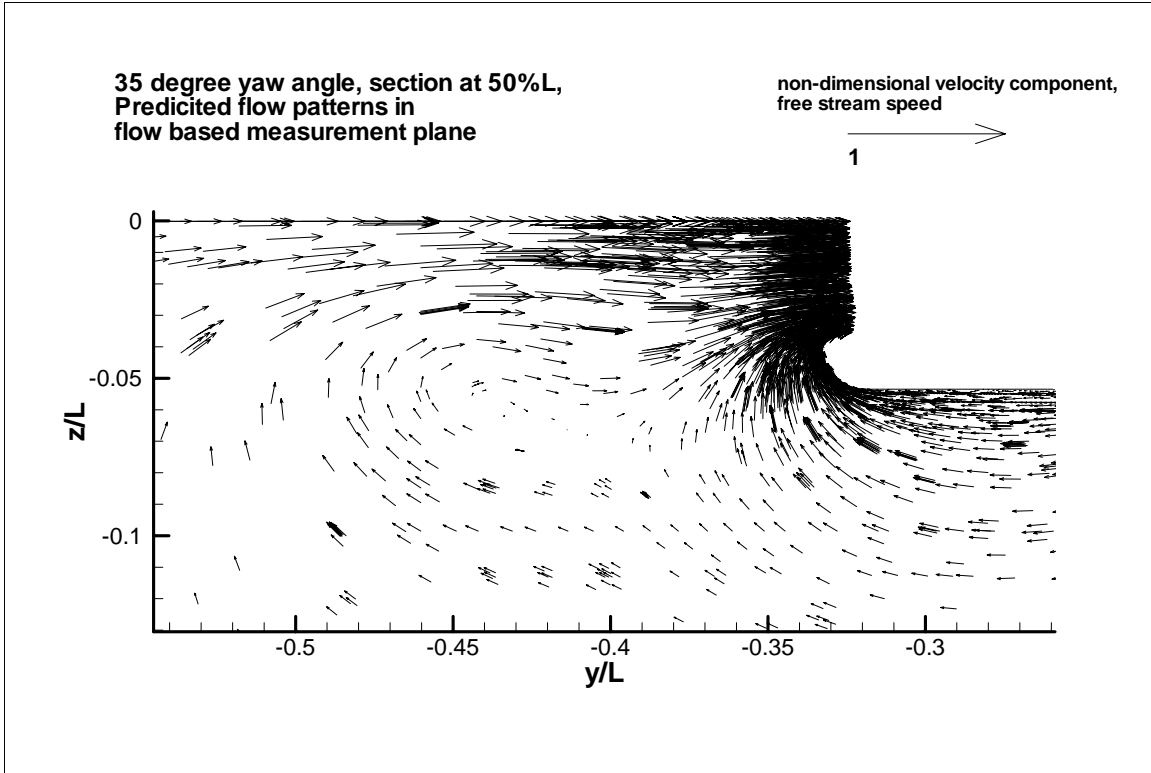


Figure 19, Tetrahedral mesh, Yaw angle 35 degrees, CFD predictions of flow patterns at $x/L=0.50$

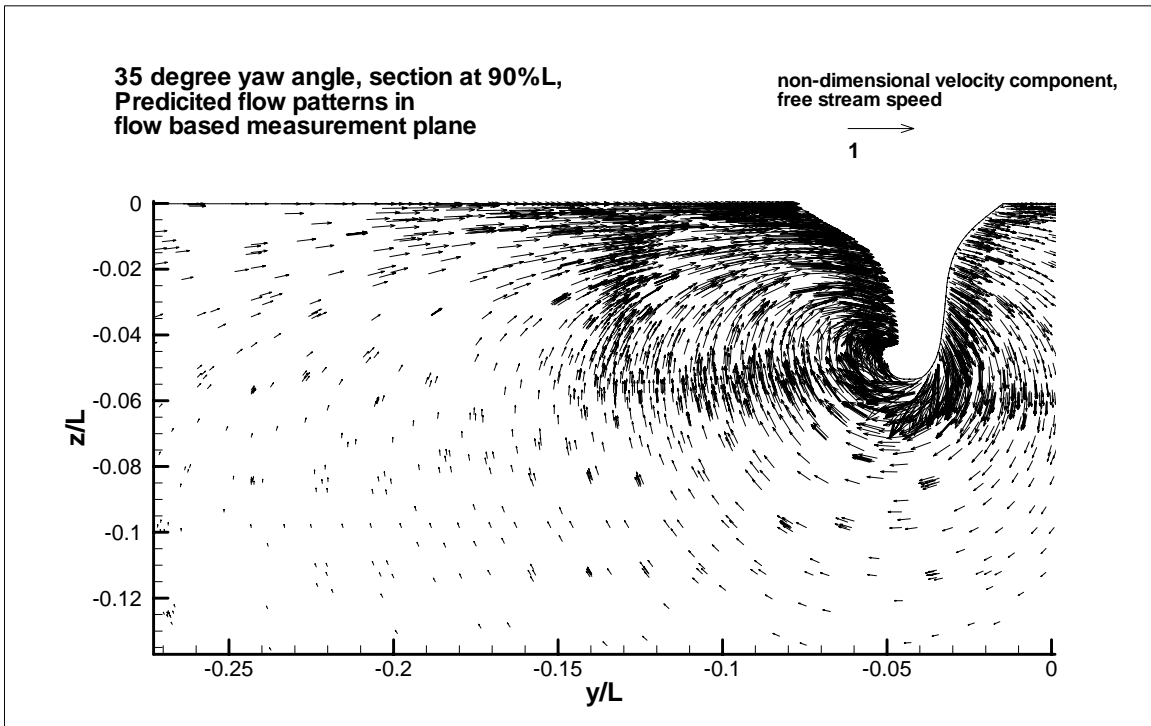


Figure 20, Tetrahedral mesh, Yaw angle 35 degrees, CFD predictions of flow patterns at $x/L=0.90$

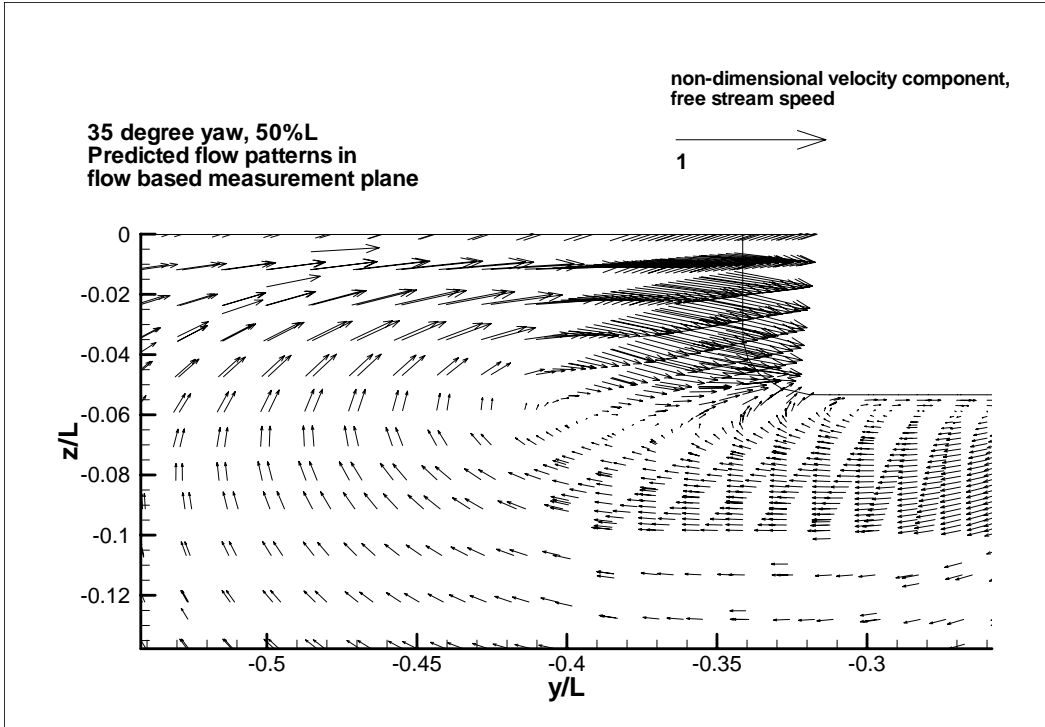


Figure 21, Hexahedral mesh, Yaw angle 35 degrees, CFD predictions of flow patterns at $x/L=0.50$

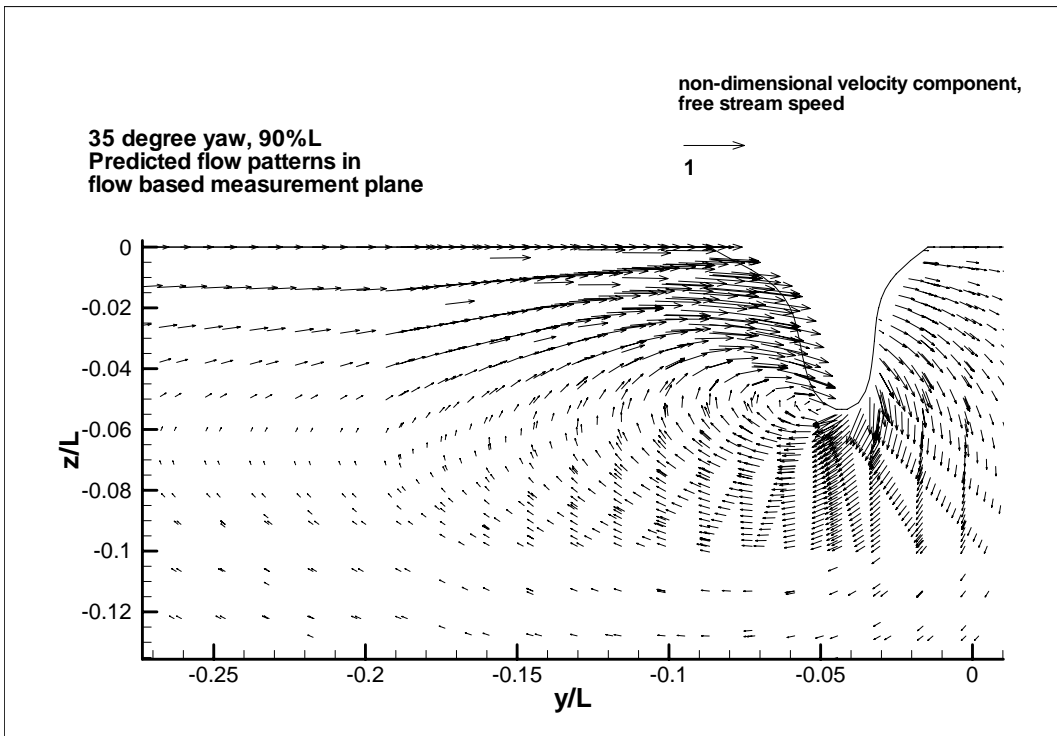


Figure 22, Hexahedral mesh, Yaw angle 35 degrees, CFD predictions of flow patterns at $x/L=0.90$

Discussion of Observed Flow Patterns

The three sections around the hull chosen for comparison between experiment results and CFD predictions were at $x/L=0.2$, 0.6 and 0.9. These represented three distinct regions within the flow. These may be broadly categorized as an entry region, in which the flow is accelerating around the hull, a midsection region, where the flow is at the maximum distortion from the free stream, and a stern region, where the flow is dominated by the wake of the hull.

Based on the results of the experiments some key features of flow patterns around a Series 60 hull with a yaw angle were observed and it is important that the CFD simulations capture these features. These observations are summarized in Table 5.

Yaw angle, deg.	Flow feature	Figure, Experiment	Figure, Tetrahedral mesh	Figure, Hexahedral mesh
10	Closed contour of u velocity component that moves from the centreline towards the downstream side of the hull as flow moves further aft along hull	3, 4, 5	13, 14, 15	16, 17, 18
10	Strong downward flow component on upstream side of hull, up to 60%L	3, 4	13, 14	16, 17
10	Strong upward flow component on downstream side of hull from 60%L to stern	4, 5	14, 15	17, 18
10	Strong circulating flow component on downstream side at 90%L	5	15	18
35	Strong circulating flow on downstream side of the hull at 50%L, which was not observed at 10 degrees	7	19	21
35	Strong circulating flow on downstream side of hull at 90%L	8	20	22

Table 5, Summary of observed flow patterns for experiments and CFD predictions

At 10 degrees yaw, both meshes capture the in-plane velocity components well, with the exception of the local region close to the vortex observed at each section. Neither of the meshes gives adequate representation of the flow around the vortex core. The hexahedral mesh however, appears to do a better job of predicting the through-plane velocity component. The contours of u for this case show greater resemblance to the experiment values along the length of the hull.

At 35 degrees of yaw, the experiment data is sparser, since only two sections were measured, and only in two dimensions. The experiment results show a strong flow towards the hull at the waterline, and a well-developed vortex shed from the keel. Both CFD predictions show these characteristics, although the flow around the vortex core is less circular than the flow observed in the experiments. Although there are some obvious local deficiencies in the flow patterns when compared to the experiments, the results of the CFD predictions capture the essential features of the flow around a hull with a yaw angle.

EVALUATION OF CFD SIMULATIONS USING DIFFERENT MESHING STRATEGIES AGAINST EXPERIMENT RESULTS

A detailed comparison of a CFD simulation with physical measurements of the same flow condition is an important step in assessing its accuracy. The methods used to make the comparison depend on the overall objectives required from the simulations. In many engineering studies, accurate predictions of the forces and moments resulting from the fluid flow around an object are a sufficient measure of the accuracy of the simulations. If the results of the CFD simulations are within the uncertainty of the experiments, then the predictions have been made with sufficient accuracy. This assessment approach is attractive since it is based on a single quantity that is significant to many engineering solutions. It is however only a partial understanding of the accuracy of the CFD prediction. A full validation includes comparing the flow patterns as well as the resulting forces.

The discussion above on the comparison between the experiment results and the CFD predictions is subjective. In order to make meaningful evaluations, a structured numerical approach is required. This section outlines the development of a method that can be used for making comparisons between experiment results and the different CFD meshes, in order to determine the most effective meshing strategy.

Development of a Numerical Evaluation Method for Comparing Flow Patterns from CFD Predictions and Experiment Results

Flow measurements for the Series 60 hull were two-dimensional LDV measurements of in-plane flow components at a yaw angle of 35 degrees and three-dimensional velocity components measured with Pitot tubes at a yaw angle of 10 degrees. Since the most generally accepted way to present the results of flow around a hull with yaw is as vectors of in-plane velocity combined with contours of through-plane velocity, this was used as the basis of the comparison, but it was recognized that three velocity components might not be available in every case. The steps in the evaluation process are described below, and where necessary they are graphically illustrated using experiment data for the Series 60 hull, from the section at $x/L=0.9$ at 10 degrees of yaw and CFD predictions for the hexahedral mesh for the same condition.

Preliminary Processing

The first step in the preliminary processing is to make the velocity components non-dimensional, by dividing by the free stream velocity. This makes all analysis relative to the free stream flow values of 1.0, and as a result interpretation of the comparisons is easier, since the results are dimensionless. Also, for PIV or LDV measurements it is necessary to remove any flow measurements at spatial coordinates inside the geometry of the hull. These data points are usually caused by reflections from the surface of the model.

Grid for Comparison of Data

A grid must be developed which is common to the experiment results and the CFD predictions. A typical experiment grid will contain far fewer points than a CFD grid, and as a result is the most likely candidate for the grid used for the evaluation, but it is possible that the experiment grid is larger than required for the comparison, or that the original spacing was not optimum.

The development of the evaluation grid can be an iterative process. If the experiment grid is very large, then there may be areas where flow measurements are close to the free stream conditions. In these cases, agreement between the experiment results and the CFD simulations should be easy to obtain, and this will bias the overall error comparison, by including a large number of points with small errors. The selection of the region for comparison is subjective, and the most appropriate area depends on the specific flow conditions being investigated. An example of a comparison grid is shown in Figure 23. In this case the grid has been reduced from the complete experiment grid, because the errors on the upstream side of the hull were very small.

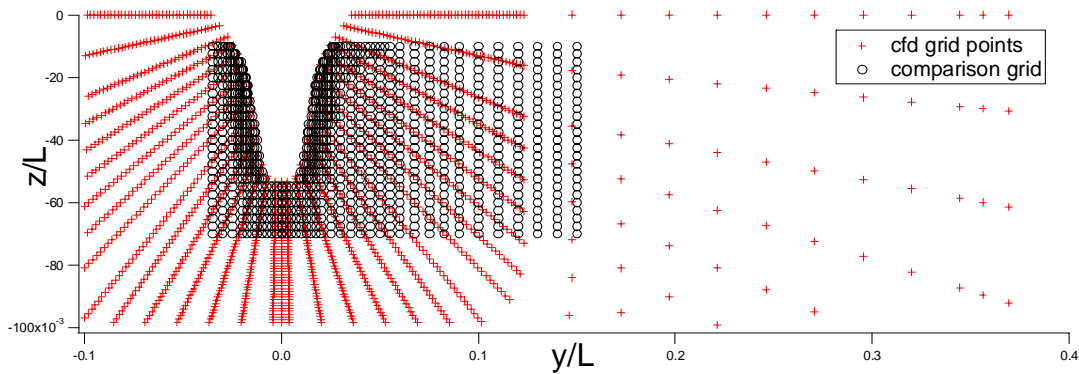


Figure 23, Comparison of CFD grid points with comparison grid

Interpolate CFD and Experiment Results on Common Grid

The three experimentally obtained velocity components in the orthogonal x , y , z planes were referred to as u_{expt} , v_{expt} and w_{expt} . The magnitude and direction of the in-plane velocity vectors were obtained by combining the v and w components.

$$|v|_{expt} = \sqrt{v_{expt}^2 + w_{expt}^2}$$

$$\theta_{expt} = \tan^{-1} \left(\frac{w_{expt}}{v_{expt}} \right)$$

Individual velocity components from the CFD solutions were plotted as contours over the complete fluid domain at the section used for comparison. The contours of single velocity component were interpolated at the points of the grid used for comparison. The resulting velocity components were u_{cfd} , v_{cfd} and w_{cfd} . Vectors of in-plane flow were calculated from the combination of v and w components.

$$|v|_{cfd} = \sqrt{v_{cfd}^2 + w_{cfd}^2}$$

$$\theta_{cfd} = \tan^{-1}\left(\frac{w_{cfd}}{v_{cfd}}\right)$$

An example of the comparison between the experiment values and the CFD predictions, plotted on the same grid is shown in Figure 24. This is for the same grid shown in Figure 23.

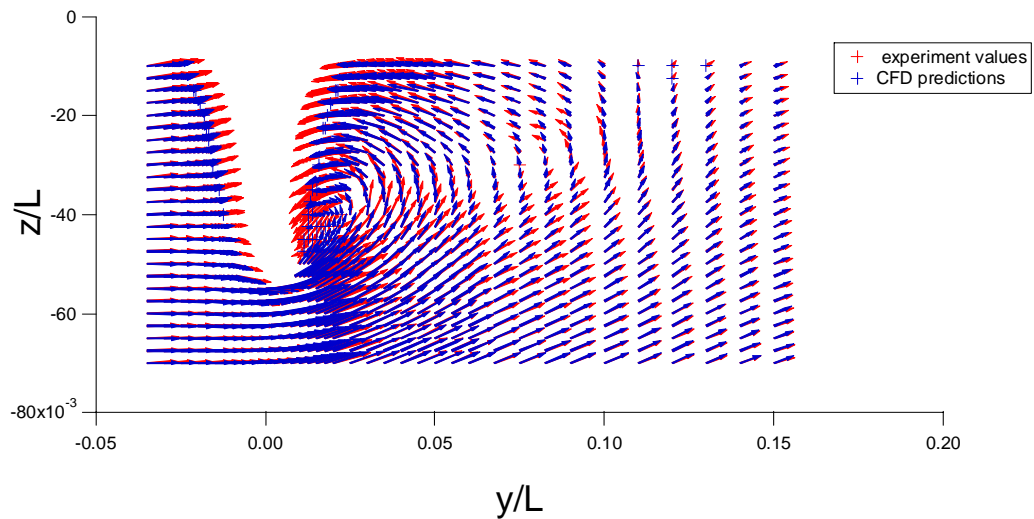


Figure 24, Comparison of in-plane vectors on common grid

An effective graphical method of presenting the error within the plane of the measurement was to subtract these two vectors.

$$\overline{V_{error}} = \overline{V_{expt}} - \overline{V_{cfd}}$$

This can then be graphed over the comparison grid. When the difference between these vectors was small, the CFD prediction was a good match to the experiment results, and when the difference was large, the CFD results were a poor fit. An example is shown in Figure 25.

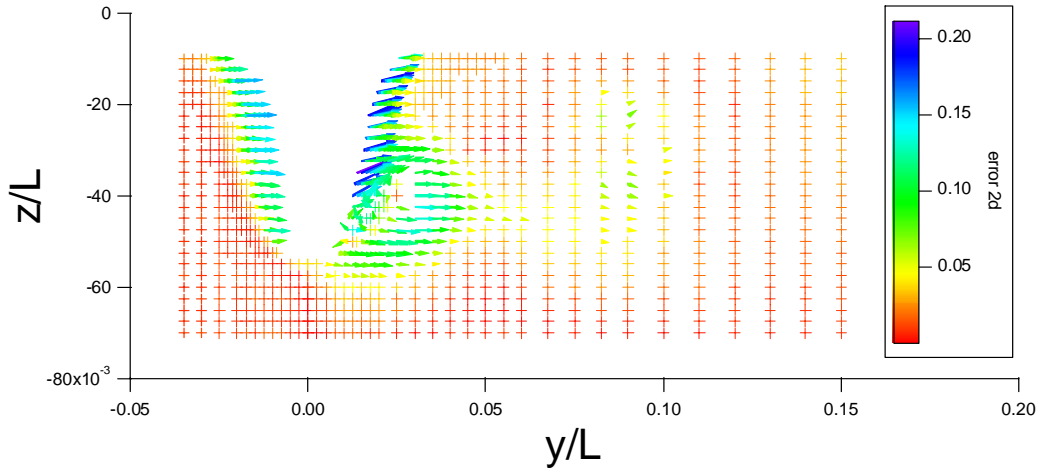


Figure 25, Error vectors for in-plane flow, coloured by two-dimensional error magnitude

The errors in magnitude and direction are both shown in this figure. The length of the arrow gives the magnitude of the error, with a small arrow corresponding to a small magnitude. If the arrow is pointing horizontally, from left to right, then there is an error in magnitude but no error in direction. As the arrow rotates away from this position, it indicates an increasing error in direction. Colour is used to put a numerical scale on the value of the magnitude of the error. Figure 25 shows that the largest errors occur very close to the hull surface and within the vortex on the downstream side of the hull.

The following parameters were also used part of the numerical evaluation of the difference between the experiment values and the CFD predictions

$$Error_u = u_{\text{expt}} - u_{\text{cfd}}$$

$$Error_v = v_{\text{expt}} - v_{\text{cfd}}$$

$$Error_w = w_{\text{expt}} - w_{\text{cfd}}$$

These parameters gave information on any bias in the flow components between the experiments and the CFD predictions. If the error was negative, then the CFD prediction was over estimating the flow speed, and if it was positive, it was under estimating. The numerical values of the mean, the standard deviation, the minimum and maximum of these components gave additional insight into the level of the match. A perfect match would have all four values as zero. This is not likely, and so the actual values of these parameters can be used to compare the different results. The better match between experiments and CFD predictions for two different grids would have the smallest mean, the smallest standard deviation, the highest minimum value and the lowest maximum value of the error components. A histogram of the velocity components can also help in interpreting the results. A histogram of the distribution of the error in the u velocity component is given in Figure 26.

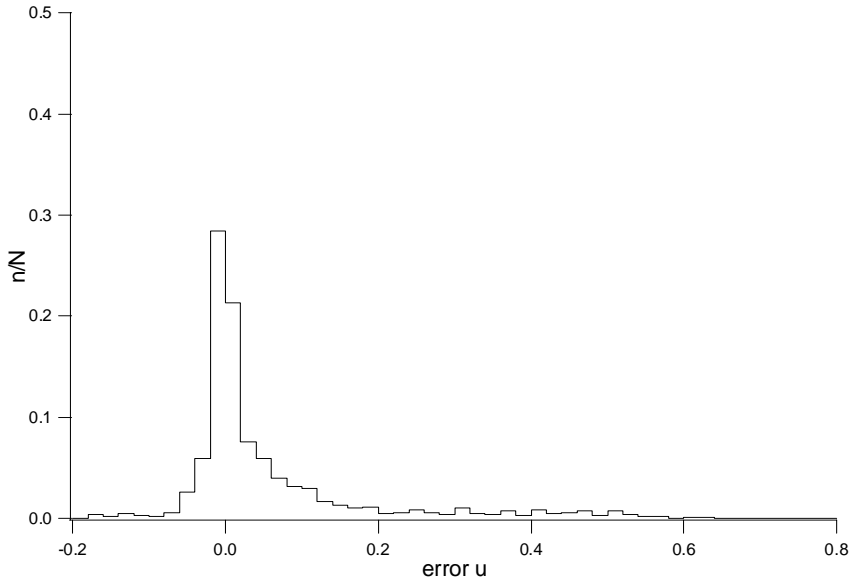


Figure 26, Histogram of error in u velocity component

Also, plotting the grid values, coloured by the error in each velocity component, can show the distribution of the error in a single velocity component over the comparison mesh. An example of this for the through-plane velocity is shown in Figure 27.

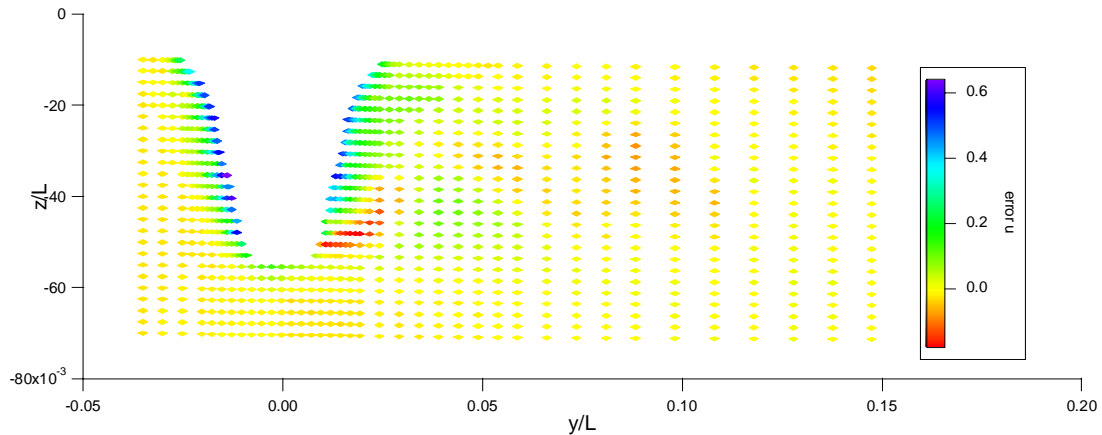


Figure 27, Spatial distribution of error in through-plane velocity

Two additional values were calculated as indications of the magnitude of the error between the experiment results and the CFD predictions.

$$Error_{2D} = \sqrt{Error_v^2 + Error_w^2}$$

$$Error_{3D} = \sqrt{Error_u^2 + Error_v^2 + Error_w^2}$$

These were found to be useful in comparing the magnitude of the error in the combined velocity components, which was not available from the individual velocity components. For example, using $Error_{2D}$ to colour the presentation of the error vector results puts a numerical scale on the magnitude of the error and enhanced the presentation of the results. Also, histograms of these parameters were found to be helpful in comparing the results from different meshes. An example of a histogram of the error of the in-flow velocity components ($Error_{2D}$) is given in Figure 28.

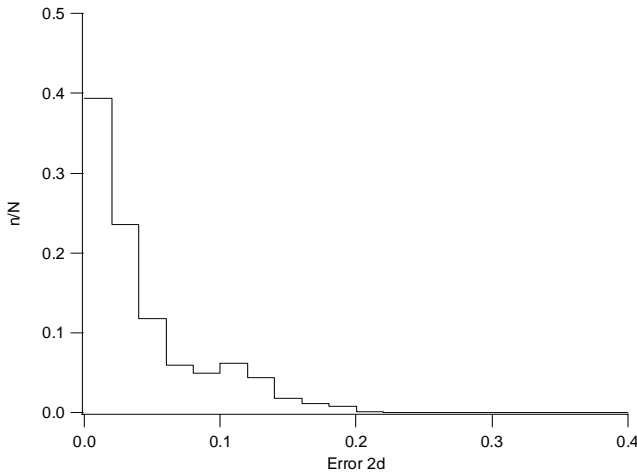


Figure 28, Histogram of error for in-plane velocity ($Error_{2d}$)

The numerical values obtained from the comparisons can be presented in a table, such as Table 6.

Hexahedral mesh					
Section at 90%L					
	Average	Standard Deviation	Minimum	Maximum	Range
In-plane velocities					
$Error_v$ (transverse component)	0.005	0.052	-0.187	0.149	0.336
$Error_w$ (vertical component)	-0.001	0.033	-0.162	0.127	0.289
$Error_{2D}$	0.044	0.043	0.001	0.211	0.210
Through plane velocity					
$Error_u$ (longitudinal component)	0.056	0.127	-0.175	0.638	0.812
$Error_{3D}$	0.091	0.122	0.004	0.655	0.650

Table 6, Example of numerical values used for error analysis

The numerical analysis and visualization of the error between the experimental values and the CFD predictions was carried out using *Igor* (Wavemetrics Inc., 2005). This is a general-purpose computer program for data analysis and presentation.

The method presented was based on comparing measured and predicted three-dimensional velocity components at a common plane within the fluid. This type of planar arrangement of the experiment data is typical of several types of experiments. PIV measurements naturally lead to this approach, where the measurement window within the fluid is a plane created by the laser sheet. LDV measurements are typically carried out in one plane, which has some relevance to the geometry of the problem. Pitot tube measurements, such as those used for wake surveys of ship models also are carried out in a similar way, although there is no need to limit measurements to points in a plane. The comparison method could be expanded to a volume comparison, but it would need several closely spaced planes of experiment data in order to make the comparison meaningful. It was assumed that if the planes were well separated (where small changes in the flow at one plane would have negligible changes in the flow at the downstream planes), then it was more meaningful to keep the comparisons to the separate planes.

ANALYSIS OF CFD PREDICTIONS USING TETRAHEDRAL AND HEXAHEDRAL MESHES FOR SERIES 60 HULL WITH YAW ANGLES OF 10 DEGREES AND 35 DEGREES

Yaw angle 10 degrees

The forces from the CFD predictions are compared with the measured values in Table 7. On the basis of force predictions alone, the tetrahedral mesh is the most accurate, and the total force given by the CFD prediction is within 5 percent of the value measured in the experiments. The hexahedral mesh has a force prediction within 14 percent of the value measured in the experiments.

Mesh	Number of Iterations	F_x, N	F_y, N	C_t*10^{-3}	C_s*10^{-3}	$C_{st}*10^{-3}$
CFD, Tetrahedral	176	4.508	13.56	$7.471*10^{-3}$	$22.474*10^{-3}$	$23.683*10^{-3}$
CFD, Hexahedral	116	3.404	15.18	$5.642*10^{-3}$	$25.152*10^{-3}$	$25.777*10^{-3}$
Model experiments				$5.35*10^{-3}$	$22.0*10^{-3}$	$22.641*10^{-3}$

Table 7, Summary of Forces from CFD predictions and model experiments

The evaluation method described above was used to compare the flow patterns predicted by the CFD simulations from the two different meshes against the results of the experiments. For the yaw angle of 10 degrees, the sections used for the comparison were $x/L=0.2$, 0.6 and 0.9. A preliminary analysis was carried out using the complete experiment grid as the basis for comparison. This analysis showed that at all sections on the upstream side of the hull, far from the model, the agreement between the CFD predictions and the experiments was very good (within 2% of the free stream flow on $Error_{2d}$). Similar agreement was found on the far downstream side of the model at sections of x/L of 0.02 and 0.06. As a result the width of the experiment grid was reduced,

so that areas far upstream and downstream, where the agreement was within 2% were not considered, and the comparison was based on a reduced experiment grid focusing on flow close to the hull.

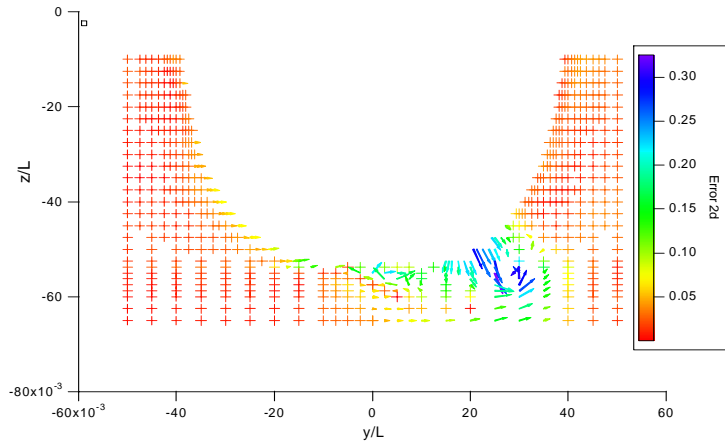
The in-plane error vectors and the through plane error for the three sections are shown in Figures 29 to 34, and summarized in Table 8.

At x/L of 0.2, the largest errors in predictions of in-plane flow for both meshes are seen around the core of the vortex at approximately y/L of 0.6 and z/L of -0.6. Outside of this region, the largest errors in the hexahedral mesh are close to the hull on both sides. This region is within the boundary layer measured in the experiments. Comparing the numerical values from Table 8, shows that the mean in-plane error magnitude is almost the same for both meshes, but the tetrahedral mesh has a slightly smaller standard deviation than the hexahedral mesh for the in-plane flow components. The hexahedral mesh has a lower error when the through plane flow component are introduced.

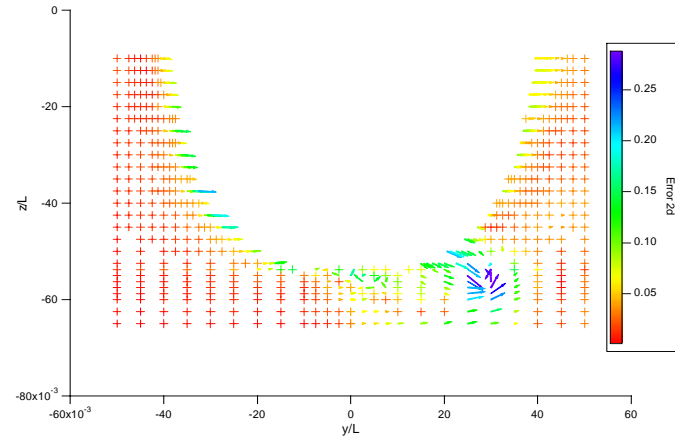
At x/L of 0.6, the largest errors are again observed around the vortex on the downstream bilge radius. The hexahedral mesh predicts the flow better in the very localized region between the vortex core and the hull but the overall average values of the in-plane error for the two meshes are almost identical, although the hexahedral mesh has a lower standard deviation. When the through-plane flow is considered, the tetrahedral mesh is more accurate than the hexahedral mesh.

At $x/L=0.9$, the evaluation of the two meshes, based on the comparison of the two CFD predictions against the experiments is more complex. The hexahedral mesh shows a better agreement with the experiment results than the tetrahedral mesh for the in-plane flow vectors, especially on the downstream side of the hull close to the waterline. For the two-dimensional comparison, the mean, standard deviation and range are all lower for the hexahedral mesh than for the tetrahedral mesh. Based on a subjective comparison of the through plane contours of velocity (Figure 15 for the tetrahedral mesh and Figure 18 for the hexahedral mesh) it looks as though the hexahedral mesh is a better predictor of the flow, since the contours on the downstream side look more like those observed in the experiments. Numerically however, when the whole comparison region was considered, the mean error in the tetrahedral mesh was lower. The only factor that is better for the hexahedral mesh was that the range, between the maximum and minimum error was reduced.

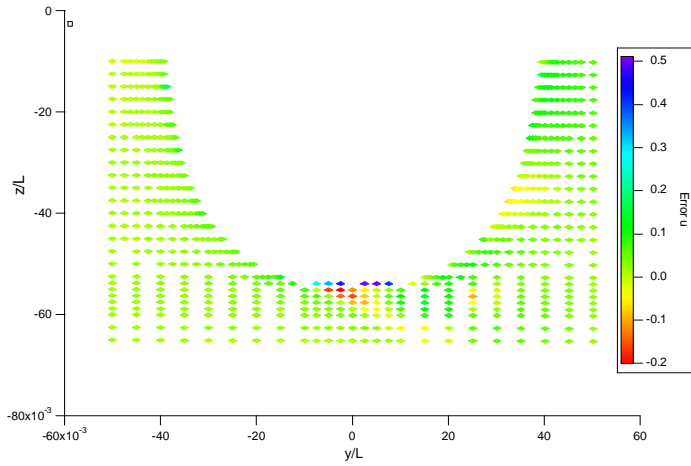
Overall, both meshes give average in plane error magnitudes of less than 5% of the free stream velocity, with the exception of the tetrahedral mesh at x/L of 0.9, where the value is less than 7%. Maximum error magnitudes for the in-plane components are between 21% and 32.5% of the free stream values, and these typically occur around the vortex core, or close to the hull, within the boundary layer for the model experiments.



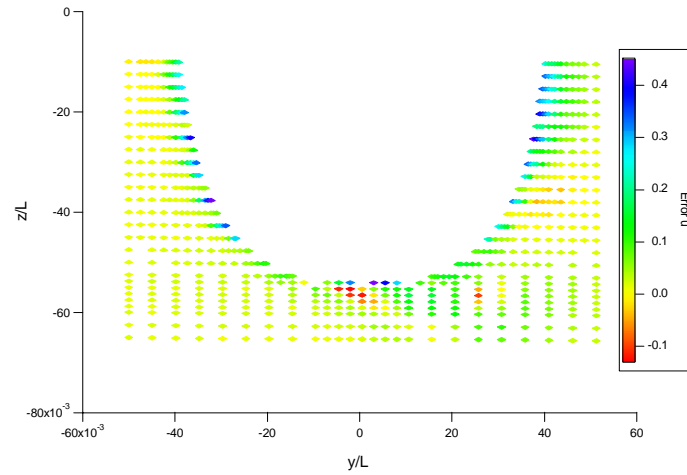
a) In-plane error



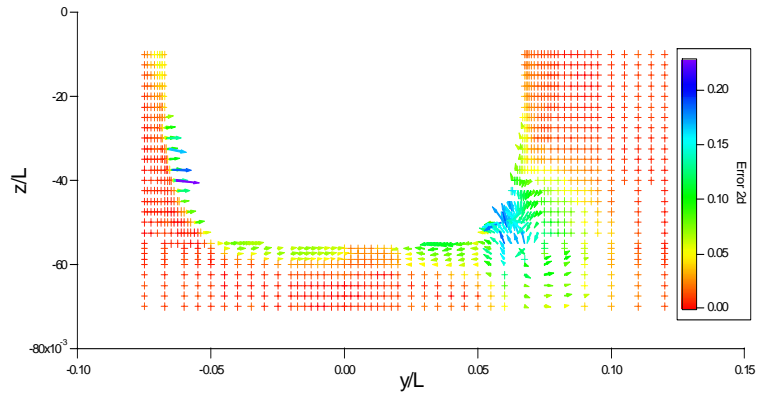
a) In-plane error



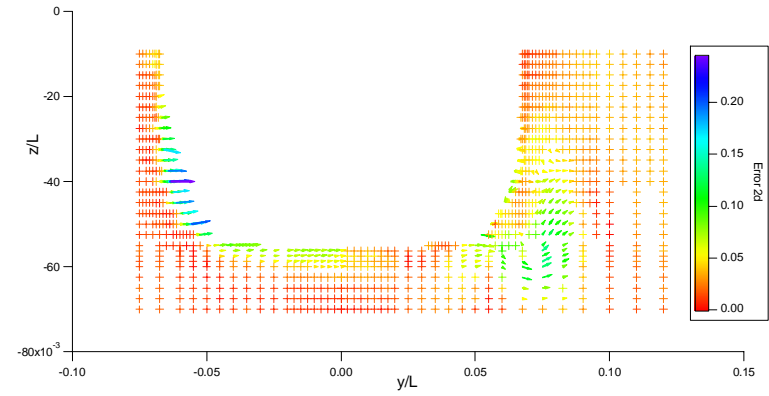
b) Through plane error
Figure 29, Section at 20%L, Tetrahedral mesh



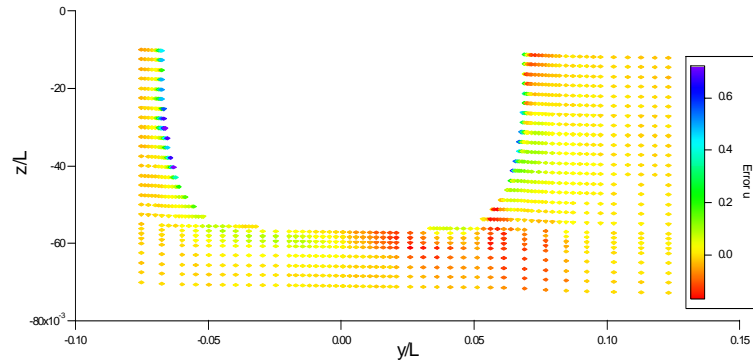
b) Through plane error
Figure 30, Section at 20%L, Hexahedral mesh



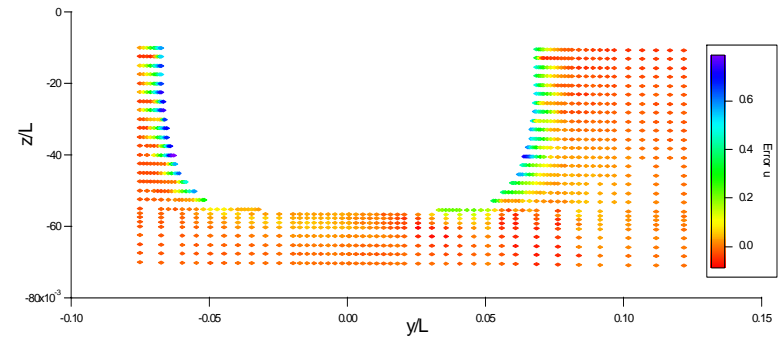
a) In-plane error



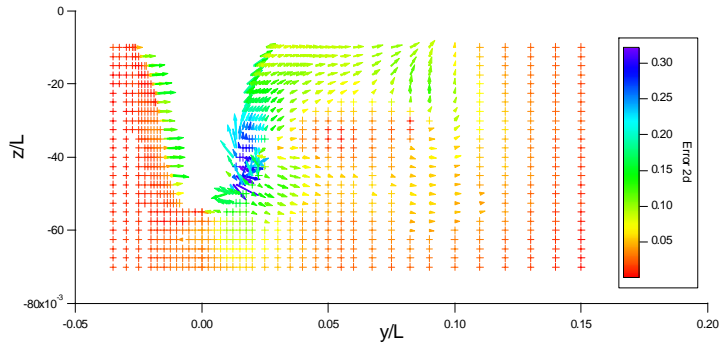
a) In-plane error



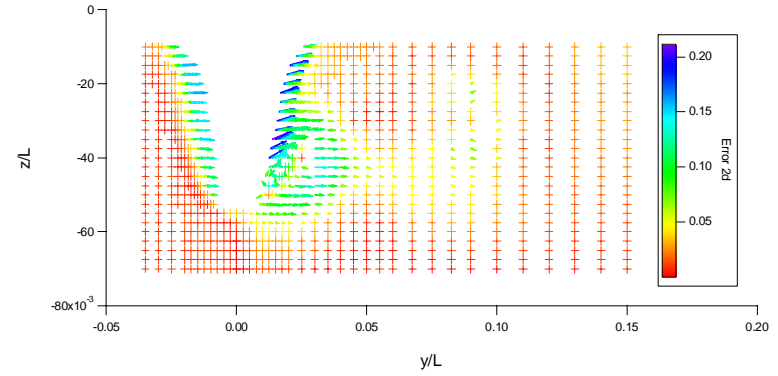
b) Through plane error
Figure 31, Section at 60%L, Tetrahedral mesh



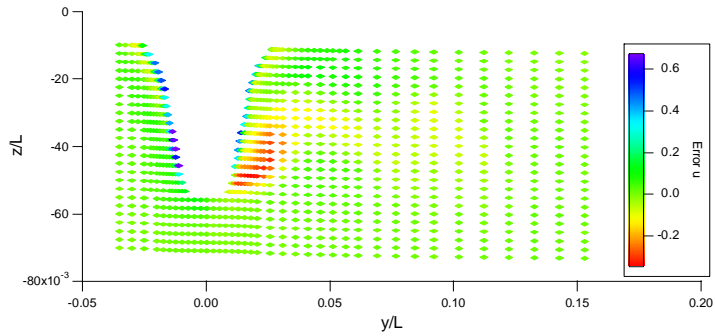
b) Through plane error
Figure 32, Section at 60%L, Hexahedral mesh



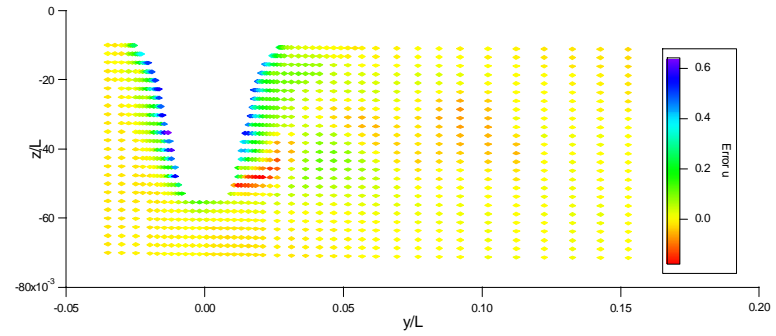
a) In-plane error



a) In-plane error



b) Through plane error
Figure 33, Section at 90%L, Tetrahedral mesh



b) Through plane error
Figure 34, Section at 90%L, Hexahedral mesh

Tetrahedral mesh Section at 20%L						Hexahedral mesh Section at 20%L					
	Average	Standard Deviation	Minimum	Maximum	Range		Average	Standard Deviation	Minimum	Maximum	Range
In-plane						In-plane					
<i>Error_v</i> (transverse component)	0.003	0.051	-0.277	0.206	0.483	<i>Error_v</i> (transverse component)	-0.008	0.057	-0.301	0.170	0.471
<i>Error_w</i> (vertical component)	-0.009	0.046	-0.243	0.285	0.528	<i>Error_w</i> (vertical component)	-0.011	0.047	-0.272	0.293	0.565
<i>Error_{2d}</i>	0.050	0.048	0.002	0.287	0.285	<i>Error_{2d}</i>	0.047	0.058	0.001	0.325	0.323
Through plane						Through plane					
<i>Error_u</i> (longitudinal component)	0.066	0.091	-0.129	0.451	0.580	<i>Error_u</i> (longitudinal component)	0.033	0.055	-0.199	0.509	0.708
<i>Error_{3d}</i>	0.093	0.094	0.007	0.495	0.487	<i>Error_{3d}</i>	0.069	0.070	0.006	0.521	0.515
Tetrahedral mesh Section at 60%L						Hexahedral mesh Section at 60%L					
	Average	Standard Deviation	Minimum	Maximum	Range		Average	Standard Deviation	Minimum	Maximum	Range
In-plane						In-plane					
<i>Error_v</i> (transverse component)	-0.010	0.038	-0.140	0.136	0.276	<i>Error_v</i> (transverse component)	0.012	0.032	-0.083	0.192	0.275
<i>Error_w</i> (vertical component)	-0.005	0.039	-0.182	0.102	0.284	<i>Error_w</i> (vertical component)	0.007	0.034	-0.194	0.134	0.328
<i>Error_{2d}</i>	0.038	0.041	0.001	0.227	0.227	<i>Error_{2d}</i>	0.039	0.029	0.000	0.244	0.244
Through plane						Through plane					
<i>Error_u</i> (longitudinal component)	0.025	0.106	-0.164	0.718	0.881	<i>Error_u</i> (longitudinal component)	0.090	0.173	-0.082	0.785	0.866
<i>Error_{3d}</i>	0.074	0.098	0.002	0.753	0.751	<i>Error_{3d}</i>	0.123	0.160	0.004	0.822	0.818
Tetrahedral mesh Section at 90%L						Hexahedral mesh Section at 90%L					
	Average	Standard Deviation	Minimum	Maximum	Range		Average	Standard Deviation	Minimum	Maximum	Range
In-plane						In-plane					
<i>Error_v</i> (transverse component)	-0.007	0.057	-0.177	0.148	0.324	<i>Error_v</i> (transverse component)	0.005	0.052	-0.187	0.149	0.336
<i>Error_w</i> (vertical component)	-0.024	0.071	-0.317	0.082	0.400	<i>Error_w</i> (vertical component)	-0.001	0.033	-0.162	0.127	0.289
<i>Error_{2d}</i>	0.069	0.064	0.002	0.320	0.318	<i>Error_{2d}</i>	0.044	0.043	0.001	0.211	0.210
Through plane						Through plane					
<i>Error_u</i> (longitudinal component)	0.006	0.113	-0.341	0.670	1.011	<i>Error_u</i> (longitudinal component)	0.056	0.127	-0.175	0.638	0.812
<i>Error_{3d}</i>	0.102	0.106	0.006	0.683	0.677	<i>Error_{3d}</i>	0.091	0.122	0.004	0.655	0.650

Table 8, Comparison data for tetrahedral and hexahedral meshes, Series 60 $C_B=0.6$ at 10 degrees of yaw

Yaw Angle 35 degrees

The forces resulting from the CFD predictions are compared in Table 9. No measured force data was available for this yaw angle. In this condition there was a very large difference in the predicted forces, but since there were no experiment values to compare with the predictions, there is no indication of which method is the most accurate.

Mesh	Number of Iterations	F_x, N	F_y, N	C_t	C_s*10^{-3}	$C_{st}*10^{-3}$
CFD, Tetrahedral	190	-3.665	-71.29	$6.074*10^{-3}$	$118.2*10^{-3}$	$118.4*10^{-3}$
CFD, Hexahedral	176	-2.660	-100.6	$4.409*10^{-3}$	$166.7*10^{-3}$	$166.8*10^{-3}$

Table 9, Summary of Forces from CFD predictions

At 35 degrees of yaw, flow patterns were measured at two sections, over a smaller region of flow. These sections were at x/L of 0.5 and 0.9. The only change to the experiment grid to make it into the comparison grid was to remove the points that were inside or very close to the surface of the hull. Also, since only in-plane vectors were measured in the experiments, the comparison with the CFD predictions was limited to the in-plane flow values only. The comparisons of the experiment results and CFD predictions are shown in Figures 35 to 38 and Table 10.

Overall, the CFD predictions for the yaw angle of 35 degrees show more error, when compared to the experiment values than for 10-degree yaw case. At 35 degrees, the average error magnitude was between 10 and 25% of the free stream velocity, with maximum error being as high as 65%. At x/L of 0.5, this larger error was mostly created by the inability of either CFD mesh to match the shape of the vortex measured in the experiments. The measured vortex was approximately circular, but in each case the predicted vortex was elongated in the y/L direction, relative to the z/L direction. At the aft section, both meshes do a better job of predicting the direction of the flow, although the magnitude of the error is still relatively high, compared to the values for a yaw angle of 10 degrees.

Based on the average error values, the flow at the aft section was predicted more accurately by both meshes than the mid section, but the maximum error was higher at the aft section. At $x/L=0.5$, the hexahedral mesh was slightly more accurate, than the tetrahedral mesh, but at the aft section, the situation was reversed.

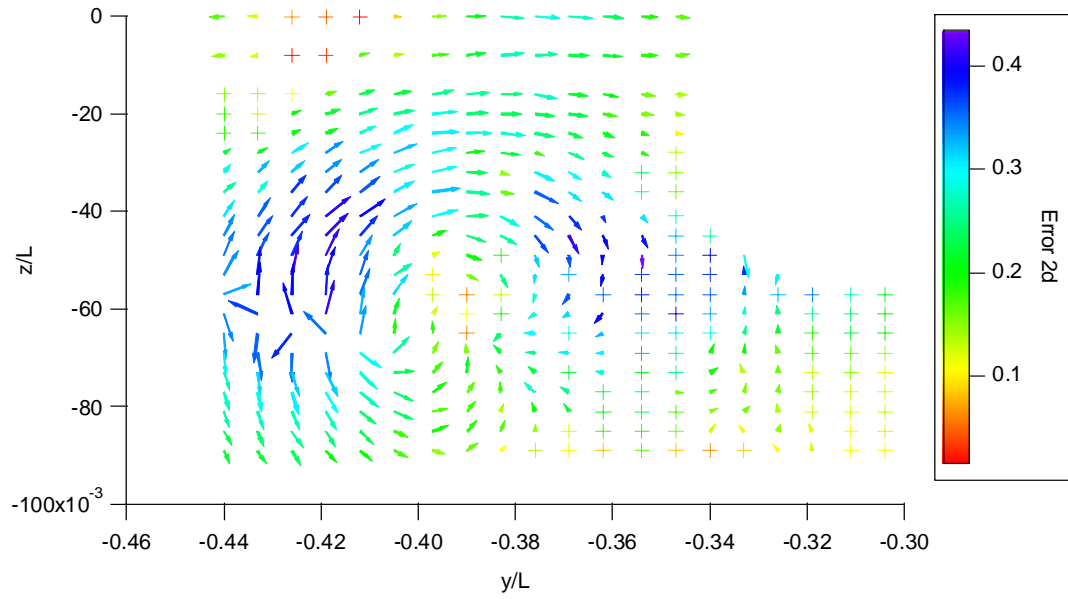


Figure 35, Section at 50% L , Tetrahedral mesh, in-plane error

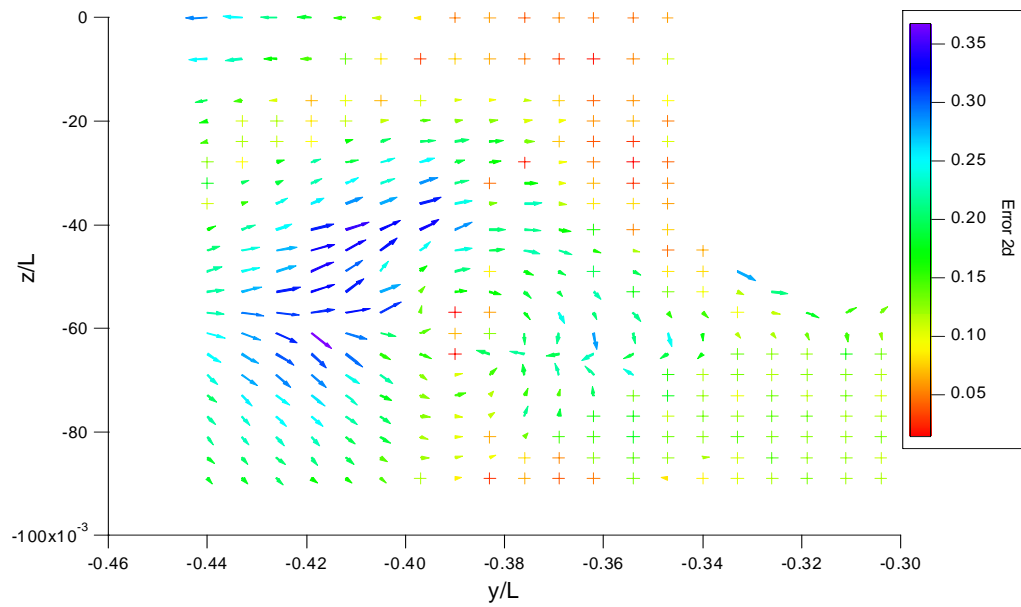


Figure 36, Section at 50% L , Hexahedral mesh, in-plane error

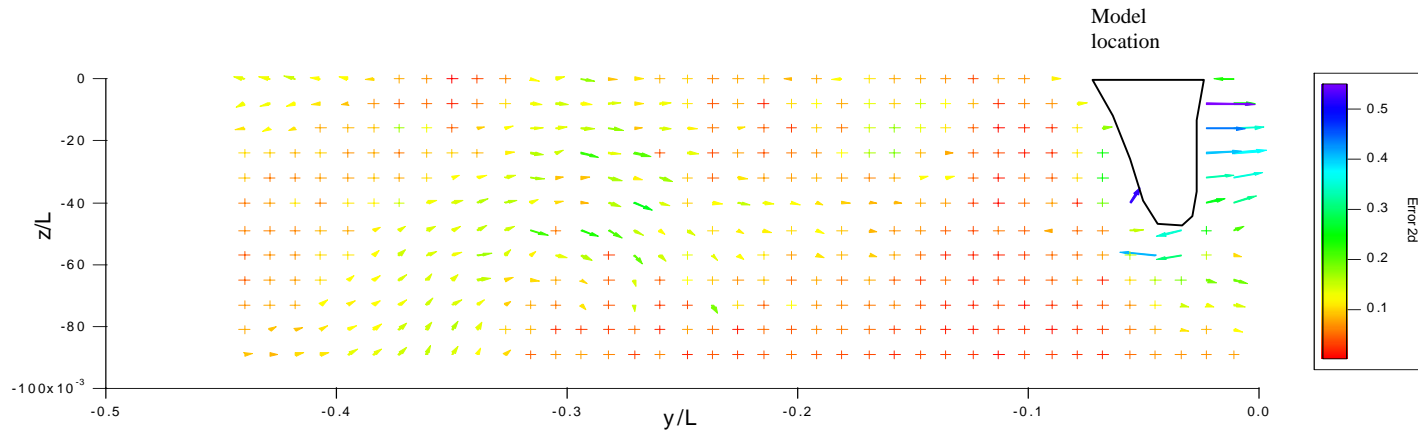


Figure 37, Section at 90% L , Tetrahedral mesh, in-plane error

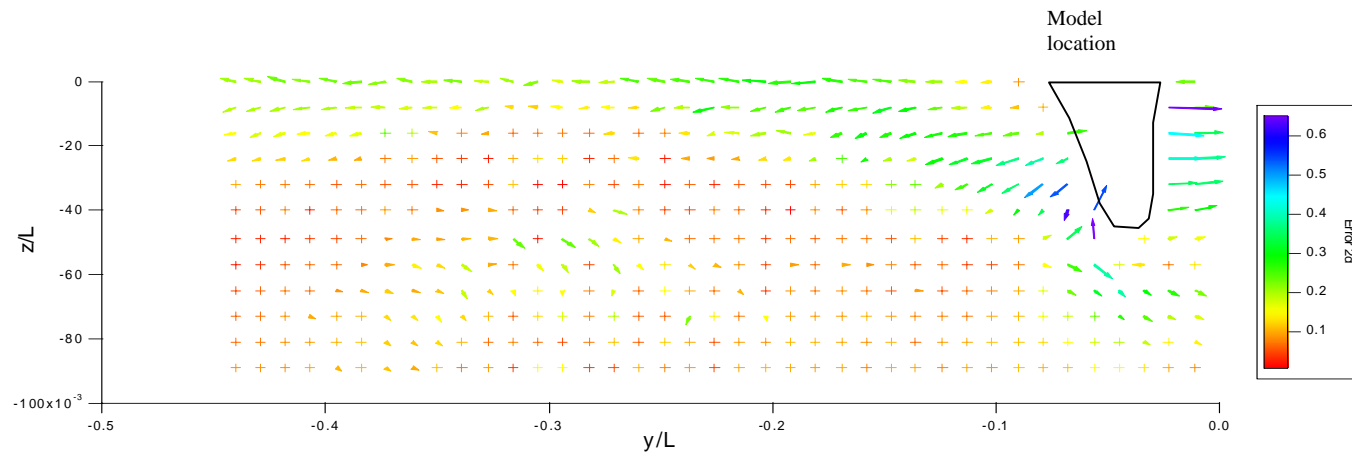


Figure 38, Section at 90% L , Hexahedral mesh, in-plane error

Tetrahedral mesh Section at 50%L						Hexahedral mesh Section at 50%L					
	Average	Standard Deviation	Minimum	Maximum	Range		Average	Standard Deviation	Minimum	Maximum	Range
In-plane						In-plane					
<i>Error_v</i> (transverse component)	0.091	0.118	-0.210	0.336	0.546	<i>Error_v</i> (transverse component)	0.053	0.096	-0.288	0.292	0.580
<i>Error_w</i> (vertical component)	0.013	0.209	-0.386	0.388	0.774	<i>Error_w</i> (vertical component)	0.049	0.135	-0.265	0.305	0.570
<i>Error_{2d}</i>	0.241	0.088	0.163	0.432	0.269	<i>Error_{2d}</i>	0.164	0.077	0.016	0.366	0.351
Tetrahedral mesh Section at 90%L						Hexahedral mesh Section at 90%L					
	Average	Standard Deviation	Minimum	Maximum	Range		Average	Standard Deviation	Minimum	Maximum	Range
In-plane						In-plane					
<i>Error_v</i> (transverse component)	0.036	0.088	-0.229	0.537	0.765	<i>Error_v</i> (transverse component)	-0.023	0.138	-0.407	0.628	1.036
<i>Error_w</i> (vertical component)	0.026	0.073	-0.169	0.513	0.682	<i>Error_w</i> (vertical component)	0.037	0.093	-0.199	0.617	0.816
<i>Error_{2d}</i>	0.102	0.069	0.004	0.548	0.544	<i>Error_{2d}</i>	0.142	0.096	0.010	0.647	0.637

Table 10, Comparison data for tetrahedral and hexahedral meshes, Series 60 $C_B=0.6$ at 35 degrees of yaw

Improvements to CFD Mesh

The main focus of this research was to investigate the effect of two different meshing strategies on the resulting forces and flow patterns for a hull with a yaw angle. This required the development and testing of numerical techniques for comparing the resulting flow patterns against the results of experiments. Generating the meshes was a necessary step in learning the details of the mesh generation program and the CFD solver but the objective of this research was not to develop fully accurate CFD predictions of flow around a Series 60 hull. Provided that the flow patterns were generally in agreement with the observed values, and that the meshes were at the point where further refinement had little effect on forces or flow patterns, then the results were considered adequate for the purposes of the comparison. A more rigorous approach would be to use the analysis methods developed here to evaluate systematically varied mesh geometries, where the effect of the number of elements and the proximity of the boundary to the ship was studied in detail.

Some refinements to the mesh may improve the accuracy of the results. Both the tetrahedral and hexahedral meshes were symmetrical about the ship centreline. Although it was not reported here, the zero yaw angle case was part of the initial study. The same mesh was used for yaw angles of zero, 10 degrees and 35 degrees. The flow direction was varied by changing the vectors at the domain boundaries, rather than rotating the hull within the domain. This resulted in the grid being fixed in relation to the geometry of the hull and not the flow conditions. One possible refinement would be to make the mesh asymmetric, so that the mesh was finer on the downstream side of the hull and in the region of the vortex generated under the hull. A further improvement would be to make the boundaries of the mesh the same as the physical boundaries of the experiment facility. Finally, using more elements at the hull surface would refine the hexahedral mesh.

For the 10 degree yaw angle case, the velocity measurements stopped below the free surface ($z/L=-0.1$) and for the 35 degree yaw angle, there was no free surface, so measured flow patterns close to the free surface were not available. Omitting the free surface will have some effect on the predicted forces and flow patterns, even at Froude numbers of 0.2 or lower. Extending the CFD predictions to include the free surface and comparing the results for the case at zero Froude number is the most obvious recommendation.

CONCLUSIONS

An evaluation method, based on numerical and graphical methods, has been developed that allowed comparisons to be made between experimental measurements of fluid velocity and predictions of the same flow conditions made using CFD. The method required the definition of an area over which the evaluation was to be made, and a grid of comparison points within this area. The user must decide on the most appropriate measurement area and grid pattern. Both of these choices will be specific for the flow patterns being studied.

Experiment values and CFD predictions were interpolated on these common grid points and numerical and graphical comparisons of the flow vectors were made. The most accurate prediction will have the smallest values for the mean error between experiments and predictions, small magnitudes for the error between the vectors and a small standard deviation of the individual velocity components. The graphical presentation shows the error in magnitude and direction between the predicted and measured vectors. The accuracy of the CFD predictions over the complete comparison area can be seen and related to the geometry of the object or key features within the flow, such as a vortex or a boundary layer.

Two CFD meshes were created for the Series 60 $C_B=0.6$ hull, one using tetrahedral elements and one using hexahedral elements. On the basis of the numerical evaluation of the flow patterns no mesh had a consistent advantage over the other for all flow conditions, if the hull was at an angle of attack to the flow. Both meshes gave more accurate predictions of flow patterns for a yaw angle of 10 degrees than for 35 degrees. If the predicted forces were included in the comparison, then at 10 degrees of yaw, the tetrahedral mesh was the most accurate. At 35 degrees yaw, the comparison can only be based on the flow patterns, and there was no clear evidence of one method being superior to the other.

Other factors, such as the time and level of skill required to create the mesh and the computational time required to come to a solution within the set tolerances can be considered in evaluating the mesh strategy. The tetrahedral mesh required a lower level of skill to create than the hexahedral mesh, although it took longer to solve a single iteration within the solution. The number of elements for the tetrahedral mesh was more than four times that of the hexahedral mesh, which was the biggest factor in determining the solution time. Even with the higher number of elements a solution for a single yaw angle and flow speed combination could be obtained overnight from the tetrahedral mesh using a PC workstation.

Based on the Series 60 hull form, for a yaw angle of 10 degrees or higher, the tetrahedral mesh is a viable strategy for meshing CFD solutions, if predicting the resulting forces and flow pattern is the primary objective. Flow patterns predicted with this mesh were just as accurate as the more commonly used hexahedral mesh. The tetrahedral meshing approach should be checked against other hull forms operating at large yaw angles, where data for forces and flow patterns are available.

ACKNOWLEDGEMENTS

I wish to thank Dr. Fabio Di Felice of INSEAN and Dr. Joseph Longo of the Iowa Institute for Hydraulic Research who provided computer files of data from their experiments, which allowed the results to be compared with the CFD predictions. In each case this required a significant effort on their part to recover and reformat the original test data, and their willingness to do this is gratefully appreciated.

REFERENCES

Alessandrini, B. A. and Delhommeau, G. 1996 'Viscous Free Surface Flow Past a Ship in Drift and in Rotating Motion', 22nd Symposium on Naval Hydrodynamics, Washington D.C., pp. 491-507.

Campana, E. F., Di Mascio, A. and Penna, R. 1998 'CFD Analysis of the Flow Past a Ship in Steady Drift Motion', Proceedings of 3rd Osaka Colloquium on Advanced CFD Applications to Ship Flow and Hull Form Design, 25-26 May, Osaka, Japan, pp. 151-159.

Cura Hochbaum, A. 1996 'Computation of the Turbulent Flow Around a Ship Model in Steady Turn and in Steady Oblique Motion', 22nd Symposium on Naval Hydrodynamics, Washington D.C., pp. 550-567.

Di Felice, F. and Mauro, S. 1999 'LDV Cross-Flow Survey on a Series 60 Double model at Incidence', Proceedings of 9th International Offshore and Polar Engineering Conference, Brest France, May 30-June 4, pp. 536-543.

Fluent Inc. 2005 'Fluent 6.2 User's Guide' available on-line, July 2005.

http://www.fluentusers.com/fluent/doc/ori/html/ug/main_pre.htm

Fluent Inc. 2005 'Gambit 2.2 User's Guide', available on-line, June 2005

http://www.fluentusers.com/gambit/doc/doc_f.htm

Löhner, R., Yang, C., Oñate, & Idelsohn, S. 1999 'An Unstructured Grid-based Parallel Free Surface Solver', *Applied Numerical Mathematics*, Vol. 31, pp 271-293.

Tahara, Y., Longo, J. & Stern, F. 2002 'Comparison of CFD and EFD for the Series 60 $C_B=0.6$ in Steady Drift Motion', *Journal of Marine Science and Technology*, Vol. 7, pp. 17-30.

Toda, Y., Stern, F. & Longo, J. 1992 'Mean-Flow Measurements in the Boundary Layer and Wake and Wave Field of a Series 60 $C_B=0.6$ Ship Model-Part 1: Froude Numbers 0.16 and 0.316', *Journal of Ship Research*, Vol. 36, No. 4. December, pp. 360-377.

Longo, J. Stern, F. & Toda, Y. 1993 'Mean-Flow Measurements in the Boundary Layer and Wake and Wave Field of a Series 60 $C_B=0.6$ Ship Model-Part 2: Scale Effects on Near-Field Wave Patterns and Comparisons with Inviscid Theory', *Journal of Ship Research*, Vol. 37, No. 1. January, pp. 16-24.

Longo, J. & Stern, F. 1996 'Yaw Effects on Model-Scale Ship Flows', Proceedings, 21st Symposium on Naval Hydrodynamics, June 24-28, Trondheim, Norway, pp. 312-327.

Longo, J. and Stern, F. 2002 'Effects of Drift Angle on Model Ship Flow', *Experiments in Fluids*, Vol. 32, pp. 558-569.

Rhee, S. H. 2005, Private correspondence by email, 11 July.

Todd, F. H. 1963 'Series 60 Methodical Series Experiments with Models of Single Screw Merchant Ships', David Taylor Model Basin Report 1712.

Turnock, S. 2006, Private correspondence by email, 7 April.

Wavemetrics Inc. 2004 'Igor Pro Version 5 Users Guide'.

Yang, C. & Löhner, R. 1998 'Fully Non-linear Ship Wave Calculation Using Unstructured Grid and Parallel Computing', Proceedings of 3rd Osaka Colloquium on Advanced CFD Applications to Ship Flow and Hull Form Design, 25-26 May, Osaka, Japan, pp. 125-150.